University of Zimbabwe

Research Topic: Mathematical modelling and performance Analysis of Solar Chimney power generation in Zimbabwe

By MAN'ARAI NDOVORWI

R014245X

Research Proposal submitted in partial fulfilment of the requirements for the degree of Master of Science in Renewable Energy, University of Zimbabwe

Supervisors:

Eng. L. Madiye And Eng. T. Hove

June 2017

ACKNOWLEDGEMENTS

This project would not have been possible without the un-tireless support and guidance received from my supervisors, Eng. T. Hove and Eng. L. Madiye. Their insightful comments and observations throughout the duration of the project is greatly appreciated.

Also, worth mentioning is the support received from fellow classmates.

Finally, and most important, my gratitude goes towards my family for the endurance and support.

Table of Contents

Tables

Abstract

This thesis analyzed the performance of a novel invention of Solar chimney power plants (SCPP) in Zimbabwe. Solar chimney power plants are based on the fundamental principle that hot air rises. The analysis was based on three locations of Kariba, Harare and Gweru.

A mathematical model that determines the solar radiation at the locations and determines the performance of a solar air collector based on the greenhouse effect was developed and used to determine the draft air velocity in the exhaust chimney.

The performance of a wind turbine was calculated and the energy generated was assessed on the ability to meet the demand of a 25KW peak community. An economic analysis was carried out on the technology and compared with the traditional wind turbine system.

It was concluded that SCPP can be developed in Zimbabwe and operated at capacity factors below those obtained if the turbines are placed in open air. The levelised cost of energy from this technology is also higher compared to ordinary wind energy systems. However, the plants can operate throughout the year.

Chapter 1:

1.1 Introduction

The use of renewable energy technology has been identified as one of the possible ways to achieve universal access to clean energy by communities in Zimbabwe (1). In 2016, the World Energy Council (2) rated Zimbabwe to have a 37% electricity access rate thus leaving a huge gap for investment in power generation to supply the marginalised rural communities. Solar PV and Wind energy power has been widely adopted in Zimbabwe. However, the intermittency nature of these resources and low capacity factor of Solar PV because of the absence of the sun at night results in huge investments in storage capacity.

Despite the invention of low cut-in wind turbines on the market as indicated in the Catalogue of low wind turbines in the European commission (3), the low wind speeds in Zimbabwe, which average 3m/s according Hove et al, 2014 (4) has made it economically impossible to use the conventional wind turbine technologies on the market to generate electricity as a result of the low capacity factor. This has been coupled by the need to import the equipment, spares and expertise for maintenance.

1.2 Background

The need to balance the energy trilemma consisting of energy security, energy equity and environmental sustainability makes Solar chimney power plants (SCPP) a possible candidate solution to electrify rural communities in Zimbabwe without grid extension. SCPP uses both solar thermal and wind energy technology to provide a 24-hour energy supply. Three major components of a solar thermal heat collector, chimney and wind turbine are required.

During daytime, the solar thermal heat collector (roof glass or plastic) heats air through the greenhouse effect. The heated air then rises through the chimney and as it passes into the chimney, it is used to turn the wind turbine, thus generating electricity.

Tamil Sakir et al in 2014 indicated that at night, ground heat and/or water filled tubes placed under the collector emit radiation that heats the air (5).

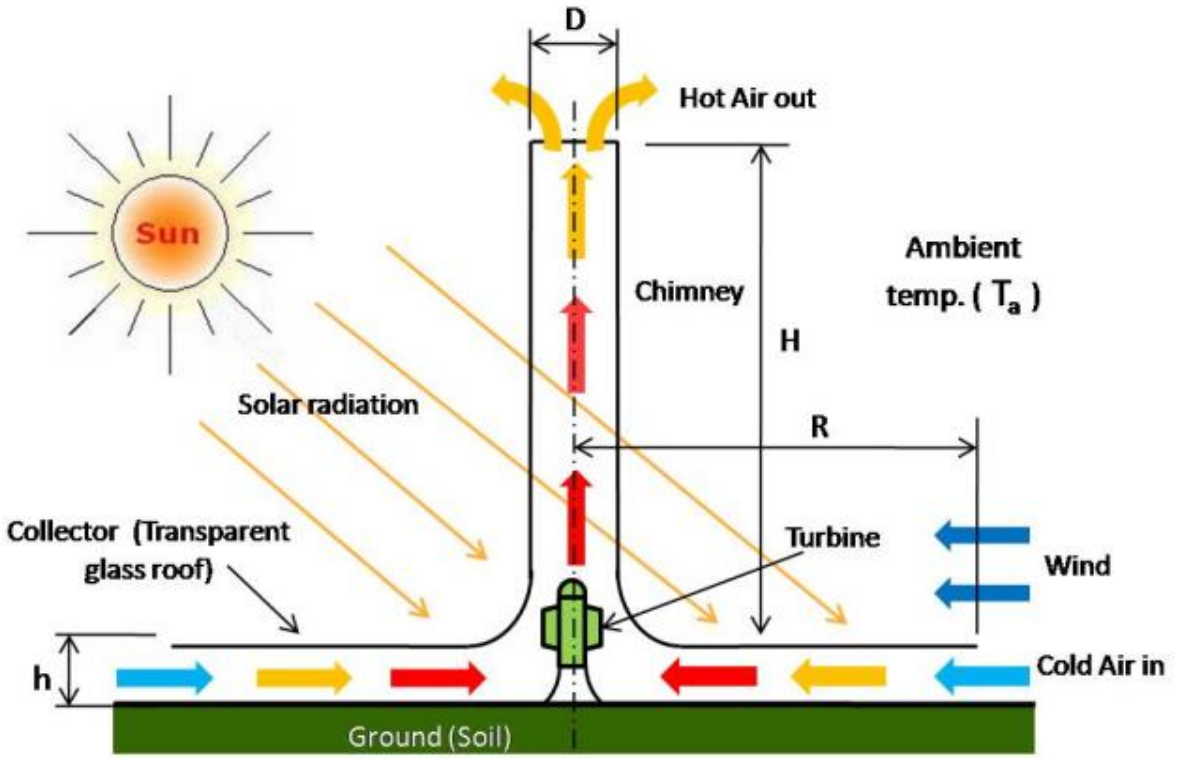

Figure 1:Diagram showing the principle of operation of a solar chimney

According to Omri et al 2013 (6) the first Solar chimney power plant was developed between 1981 and 1982 at Manzanares, Spain at a capacity of 50kW. Schlaich et al 1997 (7) give the technical dimensions of the plant as 194.6 m chimney tower, 5.08m tower radius and a mean collector radius of 122m.

Several other Solar chimney demonstration plants have been developed in China as highlighted by Fei Cao et al, 2013 (8) and in Botswana as indicated by Matsomai et al 2013 (9) and proposals are in place to have one plant in Namibia. A performance analysis of SCPP in Nigeria has indicated that between 154-181kW can be generated using a 600m collector diameter and a 150m chimney height.

An experimental test by Sakir et al 2014 (5) demonstrated that it is possible to possible to generate 3 to 20W using a chimney height of 3.05m, chimney radius of 0.076m and a solar collector radius of 2.28m.

Zimbabwe receives abundant solar radiation that exceed 2200kWh/m^2 as highlighted by Hove and Gottsche 1999 (10) making it a possible candidate for solar chimney power plants.

1.3 Problem Statement

Renewable energy power generation through Solar Chimney Power plant systems can be used to generate electricity in rural communities to support productive activities thereby improving their livelihood. However, the lack of a techno-economic feasibility of the potential of this technology in Zimbabwe has resulted in the adoption of other technologies like Solar PV which have a low capacity factor due to limited sunshine hours.

It is therefore imperative that a techno-economic feasibility study be done on the parametric size of SCPP components be selected that will provide the least cost Levelised cost of electricity (LCOE).

1.4 Justification of study

The depletion of fossil fuels and the need to combat increasing global temperatures has prompted governments to look at renewables as a sustained energy source. SCPP can be deployed as grid connected and off-grid systems reducing the huge costs incurred during grid extensions.

Two out of the three major components of SCPP, chimney tower and solar collector can be procured locally making SCPP inexpensive.

The ability of SCPP to operate continuously throughout the day reduces the amount of battery storage required when compared to standalone Solar PV and Wind systems.

It is therefore imperative that a study be undertaken to establish the operating parameters of SCPP when subjected to local irradiation conditions.

Furthermore, a comparison of SCPP system against Solar PV system needs to be done to assess whether investments in SCPP makes economic sense for off-grid systems or whether a hybrid solution will provide the much-needed energy supply for rural communities.

1.5 Research Questions

i. Is SCPP power generation feasible in Zimbabwe?
ii. Can SCPP systems be used in rural Zimbabwe to improve the rate of electrification?
iii. How much does it cost to put up a SCPP system in Zimbabwe?
iv. Do investments in SCPP generation make economic sense when compared to other renewables like solar PV?
v. How best can SCPP generation be adopted in Zimbabwe e.g. standalone system or hybrid?

1.6 Research Objectives

The objective of the thesis is to assess the feasibility of using SCPP generation in Zimbabwe. The study will also assess the cost implications of installing such systems and the best possible way of integrating SCPP systems and other renewables to achieve a lost levelised cost of energy (LCOE). The following tasks will form the basis for the research:

a. To determine the optimum size and shape of the solar collector, chimney height and diameter to meet the demand of 25kW.

b. To assess the solar radiation incident at three selected sites that have the highest, medium and lowest solar radiation in Zimbabwe.

c. To assess the thermal performance of SCPP when used in at these sites. Parameters such as capacity factor, hourly energy output and efficiency of the system will be used as an indicator for suitability.

d. To compare the performance of a SCPP wind turbine against the performance of the same turbine in open air.

1.7 Summary Methodology

The study involves identifying existing mathematical models and/or develop a mathematical model than can be used in Zimbabwe to design SCPP. This entails developing mathematical models for the solar collector, chimney, wind turbine and wind flow within the chimney.

For the solar collector, an analysis of a single cover air heater made of glass or plastic and the ground as the back plate will be evaluated in terms of radiative and convective heat transfer as well as the overall loss coefficient, the overall temperature gain within the collector and the heat transfer to the air mass and finally the air movement.

The optimum chimney height, diameter and optimum position of the turbine within the chimney will be determined. Pressure variations in the chimney are critical to establish air movement and eventually energy output.

The turbine will then be assessed its performance under four scenarios as follows;

i. The capacity factor of the turbine.
ii. The total energy generated annually.
iii. Ability to supply an off-grid community with a defined load profile. The load profile will be extrapolated from the national demand profile.

Additional assessment criteria will be the cost and size of battery storage capacity that needs to be installed for a continuous power supply.

1.8 Assumptions and Limitations

The following assumptions have been made

i. The airflow within the chimney is directly related to the radiation absorbed by the solar collector and is independent of the wind flow at the respective sites.

ii. The load profile of the country will be normalised to reflect the load profile of the off-grid community based on the economic activities being under taken. Off-grid systems such as Chependeke and Nyafaru have a capacity of 23kW and 20kW respectively.

iii. Solar radiation data for the chosen site will be based on meteorological data available. However, this will be verified by mathematical models.

Chapter 2:

2.1 Introduction

The solar chimney power plant technology works on two principles which are Greenhouse effect and buoyancy effect per Upadhyay et al 2014 (11). It is derived from the general principle that warm air rises above cold air. Using glass or plastic material, air is heated under the collector transparent roof and becomes lighter. It is then sucked by the chimney tower to be exhausted whilst cold air moves from the periphery to replace the hot air. This creates a continuous movement of air according to Bergermann and Schlaich 2011 (33). The kinetic energy in the updraft is converted to mechanical energy and electrical energy by pressure-staged wind turbines placed within the chimney.

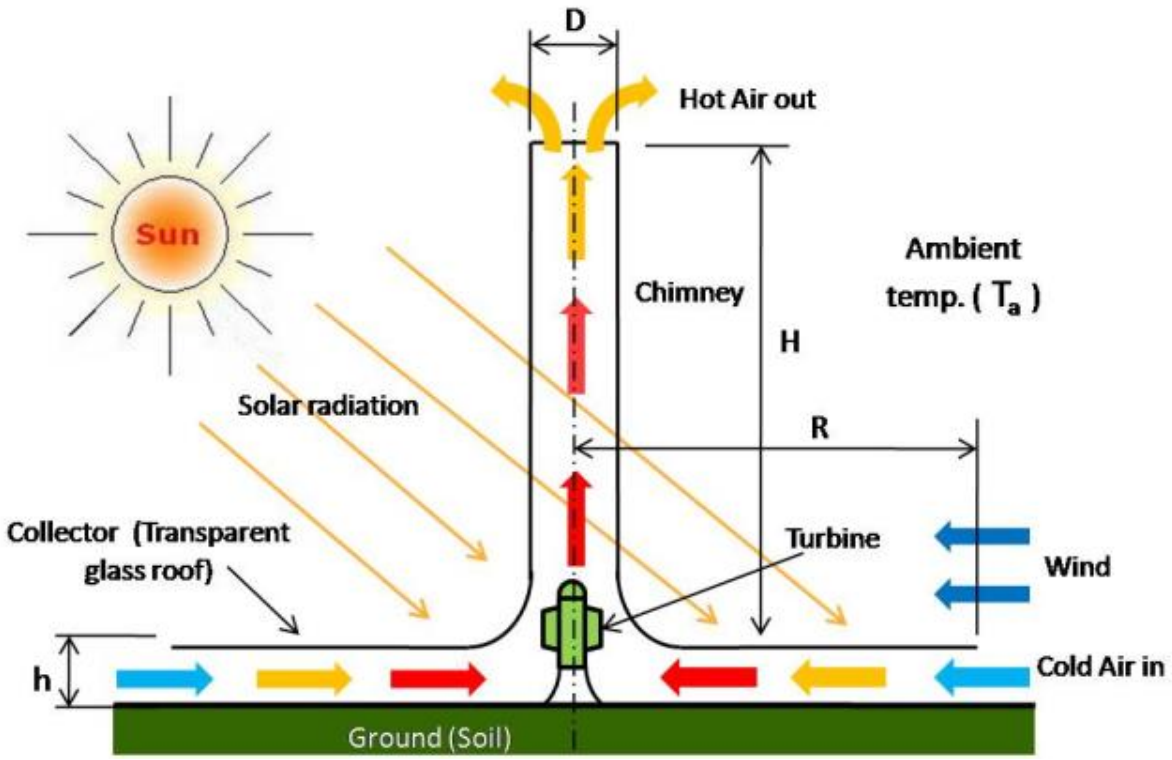

Figure 2:Operating principle of SCCP (M. Ali)

2.2 Review of Solar chimney generation technology

Dhahri and Omri 2013 (6) reviewed the solar chimney generation technology. It was revealed that the idea to use solar chimneys was first postulated in 1903 by Isodoro Cabanyes. In 1926 Prof Bernard Dubos made a proposal to construct one plant in North Africa but it never materialised. The first prototype of the technology studied by Schlaich et al 1997 (7), was constructed at Manzanares, Spain comprising of 50kW using a 194.6 m chimney tower, 5.08m tower radius and a mean collector radius of 122m.

Figure 3: Solar chimney power plant at Manzanares, Spain

Several studies have been made to this technology. Hamdan 2010 (12) analysed the performance of the solar chimney in the Gulf region using a mathematical model. The results of the model were compared with experimental data from published works. The model showed good correlation to existing results with a 3% discrepancy.

Bilgen and Rheault 2005 (13) developed a simplified computer simulation model that was used to determine the design parameters of a 5MW plant for Ottawa, Winnipeg and Edmonton. Results of the model indicated that the annual electricity production in high latitude areas is low. However, 85% more energy can be produced in favourable regions.

Omri et al (6) report that in 2010, a 200kW solar chimney plant was developed in Jinshawan, Mongolia. The project is expected to upscale to 27.5MW with a collector area covering 277 hectares at an estimated cost of US$ 208 million.

Thakre et al 2013 (14) reviewed various research models and incorporated the losses that are involved in the system making it possible to accurately predict the solar chimney power plant.

Bansod et al 2014 (15) outlined the developments in solar chimney technology. Model developments have been proposed in North America , Egypt, Nigeria, UAE, Thailand, China, and Algeria. However, no physical plant has been commissioned to date.

Figure 4:Small scale solar chimney plant prototype

The absence of a large scale commercial plants has not been feasible due to lack of financial support because of the unproven technology and high initial capital cost per Motsamai et al 2013 (9).

2.3 Theoretical mathematical models

2.3.1 Incident Solar radiation in Zimbabwe

The solar chimney technology is dependent on the solar radiation incident on the collector. It therefore follows that the number of daylight hours for a place have a

bearing on the performance of the plant. Duffie and Beckman 2013 (16) defined the average monthly days:

Table 1: Monthly average days

Month	**Day**	**Month**	**Day**
January	17	July	17
February	16	August	16
March	16	September	15
April	15	October	15
May	15	November	14
June	11	December	10

Source Klein 1977

Using the above days, the declination angle can be computed using:

$$B = (n-1)\frac{360}{365} \qquad \text{…….(}\textit{equation 1}\text{)}$$

Duffie and Beckman (16) showed that the monthly average extra-terrestrial radiation on a surface is given by:

$$\overline{H_o} = \frac{24*3600G_{sc}}{\Pi}\left(1 + 0.033\cos\frac{360n}{365} * \left(\cos\Phi\cos\delta\cos w_s + \frac{\Pi w_s}{180}\sin\Phi\sin\delta\right)\right)$$

…….(*equation 2*)

Where Φ is the latitude, n is the day number and δ is the declination angle is given by Spencer as:

$$\delta = \frac{180}{\Pi}(0.006918 - 0.399912\cos B + 0.07020257\sin B - 0.006758\cos 2B +$$

$$0.000907\sin 2B - 0.002697\cos 3B + 0.00148\sin 3B \qquad \ldots\ldots \textit{(equation 3)}$$

And $w_s\ is\ the\ sunset\ hour\ angle = -\tan\Phi\tan\delta$

The Erbs correlation as given by Duffie and Beckman (16) will be used to calculate the ratio of the monthly average diffuse radiation to the daily diffuse as given by:

$\frac{\bar{H}_d}{H} = 1.391 - 3.56\bar{K}_T + 4.189\bar{K}_T^2 - 2.137K_T^3$ for $w_s \leq 81.4^o$ and $0.3 \leq \bar{K}_T \leq 0.8$

$\frac{\bar{H}_d}{H} = 1.311 - 3.022\bar{K}_T + 3.427\bar{K}_T^2 - 1.821K_T^3$ for $w_s > 81.4^o$ and $0.3 \leq \bar{K}_T \leq 0.8$

The monthly average clearness index $\bar{K}_T$ is the ratio of the monthly average daily solar radiation on the ground to the monthly average extra-terrestrial radiation as given by Duffie and Beckman (16).

Per Hove and Gottsche 1999 (10), the ratio of diffuse radiation to the horizontal radiation for Bulawayo was approximated to:

$\frac{\bar{H}_d}{H} = 1.0294 - 1.144\,\bar{K}_T$ for $0.47 \leq \bar{K}_T \leq 0.75$

$\frac{\bar{H}_d}{H} = 0.175$ for $\bar{K}_T > 0.75$

Models to analyse the average radiation incident on a tilted solar collector have evolved from a basic sum of beam and diffuse radiation as suggested by Hottel and Woertz in 1942 to the isotropic diffuse model by Liu and Jordan in 1963 that combines bean, diffuse and ground reflected radiation as shown by the equation (16):

$I_T = I_b R_b + I_d\left(\frac{1+\cos\beta}{2}\right) + I\rho_g\left(\frac{1-\cos\beta}{2}\right)$ ……. (5)

$\bar{H}_T = \bar{H}_b R_b + \bar{H}_d\left(\frac{1+\cos\beta}{2}\right) + \bar{H}\rho_g\left(\frac{1-\cos\beta}{2}\right)$ ……. (6)

2.3.2 The collector

The collector is an air heater defined by Zhou et al 2009 (17) were ambient air at temperature T_a is heated and increases its temperature to T_c in accordance to the energy balance equation:

$$GA_{coll}\eta_{coll} = \dot{Q} = \dot{m}C_p\Delta T \quad \ldots\ldots\ldots \quad (7)$$

where G is the incident solar radiation on to the collector, A_{coll} is the area of the solar collector, η_{coll} is the efficiency of the collector, $\dot{m}$ is the mass flow rate of the heated air, C_p heat capacity of air and ΔT is the change in temperature between T_a and T_c. However, $\dot{m}$ can be found by:

$$\dot{m} = \rho_c A_c U_{in} \quad \ldots\ldots\ldots \quad (8)$$

Where ρ_c is the density of air at the collector outlet into the chimney, A_c is the cross section of the chimney and U_{in} is the velocity of air at the collector outlet.

A mathematical model and performance analysis of unglazed transpired solar collectors by Kumar and Leon 2007 (18) used the energy balance equations for the various components of the air heater system which include the absorber plate, air in the collector called the plenum air and the back plate. For the absorber plate, the energy balance equation is defined as:

$$m_c * C_p * \frac{dT_p}{dt} = (\alpha_c * I_T * A_s) - (Q_{c,c-a} + Q_{r,c-bp} + Q_{r,c-s})$$

Where $Q_{c,c-a}$ is the convective heat gain from the collector front and back plates to the plenum air, $Q_{r,c-bp}$ is the radiative heat transfer between the absorber and the back plate and $Q_{r,c-s}$ is the radiative heat loss from the absorber to the surrounding.

The heat gain by the plenum air can be derived from the following equation:

$$(m_{air-out}dt) * C_{p,air} * \frac{dT_{air,out}}{dt} = Q_{c,c-a} + Q_{c,a-bp}$$

Where $Q_{c,a-bp}$ is the heat transfer between the back plate and air.

The back-plate energy balance is defined as:

$$m_{bp} * C_{p,bp} * \frac{dT_{bp}}{dt} = Q_{c,a-bp} + Q_{r,c-bp} - Q_{c,bp-a} - Q_{r,bp-s})$$

Thakre et al 2013 (14) derived the mass flow rate in terms of the ambient air temperature and temperature rise given by:

$$m = \frac{\rho_a A_i (2gh_o \Delta T_i T_a)^{\frac{1}{2}}}{\Delta T_i + T_a} \qquad \ldots\ldots\ldots \qquad (9)$$

Where A_i is the entrance area of the chimney, h_o is the height of the chimney entrance above ground and T_a is the ambient temperature.

Ong 2002 (19) determined the volumetric air flow rate from a room as:

$$\dot{V}_o = C_d * \frac{A_o}{\sqrt{(1+A_r)}} * \sqrt{\frac{2gL(T_f - T_r)}{T_r}}$$

Where T_f, T_r are the temperature for the air flow and room temperature.

Thus, the air mass flow rate can be derived as

$$\dot{m} = C_d * \frac{\rho_{f,o} A_o}{\sqrt{(1+A_r)}} * \sqrt{\frac{2gL(T_f - T_r)}{T_r}}$$

The air density per the National Physics laboratory can be calculated using:

$$\rho_a = \frac{[(0.348444P) - h(0.00252t - 0.020582)]}{(273.15 + t)}$$

Where p is air pressure, h is relative humidity of the air and t is the air temperature

Sakir et al 2014 (5) assume a circular collector whose net energy gain from the sun is given by:

$$Q_{solar} = I * A_{coll} = \frac{I * \Pi * D_{coll}^2}{4}$$

The air movement from the collector into the chimney and out at the top of the chimney is because of pressure difference per Sakir et al 2014 (5) given by

$$\Delta p_{tot} = g * \int_0^H (\rho_o - \rho_i) dH \ = g((\rho_o - \rho_i) H_t$$

Where H_t is the height of the chimney, ρ_o, ρ_i are the air density at ambient and collector temperatures. It was further revealed that the air mass flow rate is given by:

$$\dot{m} = \rho_i * \frac{\Pi * D_t^2}{4} * V_t \text{ and}$$

$$V_t = \sqrt{\{2gH_t}(\frac{T_i - T_o)}{T_o}\}$$

Ong 2002 (19) determined the thermal network for a wall type solar chimney supplying a room and came up with three equations using the network below that define the temperature of the glass collector T_g, the collector wall T_w and the air low T_f as shown below:

$$T_g: S_1 + h_{rwg}(T_w - T_g) + h_g(T_f - T_g) = U_t(T_g - T_a)$$

$$T_f: h_w(T_w - T_f) = h_g(T_f - T_g) + \dot{q}"$$

$$T_w: S_2 = h_w(T_w - T_f) + h_{rwg}(T_w - T_g) + U_b(T_w - T_r)$$

Marquez et al 2016 (20) indicated that up to 10-15 m deep, ground heat and temperature will be as the result of the sun, thereafter, the internal thermal energy of the earth is causes an increase in underground temperature by about 3ºC for every 100m.

Kalogirou and Florides (21) indicated that the temperature of the earth is insensitive to variation in ambient temperature at depth of 1 meter and that the annual fluctuations of ground temperature extends to depth of between 9 to 12 meters.

Thereafter, the same temperature increase as predicted by Marquez et al 2016 (20) is assumed.

According to Kusada 1965 (22), the temperature of the ground depends on the time of the year as well as the depth from the surface to which the measurement is done. The following formula was given:

$$T = T_{mean} - T_{amp} * \exp\left\{-z * \sqrt{\frac{\Pi}{365 * a}}\right\} * \cos\{\frac{2\Pi}{365} * \left[t_{year-} t_{shift} - \frac{z}{2} * \sqrt{\frac{365}{\Pi * a}}\right]\}$$

Where T is the soil temperature, T_{mean} is the mean surface temperature (average air temperature. This can be assumed to be the ground temperature at infinite depth, T_{amp} is the amplitude of the surface temperature where the maximum and minimum temperatures are given by $T_{mean} + T_{amp}$ and $T_{mean} - T_{amp}$ respectively.

Z is the depth, α is the thermal diffusivity of the soil, t_{year} is the current time under consideration and t_{shift} is the day of the year when minimum surface temperature occurs.

According to Bernardes et al 2003 (23), the ground heat transfer coefficient is given by:

$$U_b = \frac{2 * \sqrt{k\rho C_p}}{\sqrt{\Pi t}}$$

Where k is thermal conductivity of the soil, ρ is the air density, C_p is the specific heat capacity of the soil and t is time.

An intensive study by Islam et al 2015 (24) that spanned 10 years of recorded data indicated a strong correlation between ambient temperature and soil temperature to

within 20cm depth. Various linear relationships were derived at 5, 10 and 20cm as follows:

At 5cm depth: y = 3.83 + 0.9x

At 10cm depth: y = 6.224 + 0.842x

At 20cm depth: y = 9.871 + 0.708x where y is the ground soil temperature and x is the ambient temperature.

According to Kurpaska 2014 (25), heat is transferred from the top glass cover of a greenhouse through radiation and convection. The convective radiation depends on the cover temperature and the ambient temperature whilst the radiative transfer is between the cover temperature and the sky temperature. According to Lin et al, sky temperature can be derived from the expression:

$T_n = 0.0522T_a^{1.5}$

Where T_a is the ambient temperature

Duffie and Beckman 2013 (16), highlighted the radiative heat transfer between the cover and the sky is then given by:

$$h_{c-s} = \frac{\sigma \epsilon_{c(T_c^4 - T_n^4)}}{T_c - T_n}$$

Where $T_c \; and \; T_n$ are the collector cover and the sky temperatures, $\sigma \; and \; \epsilon_c$ are the Stefan-Boltzman constant ($5.67*10^{-8}$ $W.m^2.k^{-4}$) and the emission coefficient of the glass cover.

The radiative heat transfer between the cover and the sky is given by Duffie and Beckman 2013 (16) as:

$$h_{r,c-s} = \frac{\sigma \epsilon_c (T_{c2} + T_s)(T_{c2}^2 + T_s^2)(T_{c2} - T_s)}{T_{c2} - T_a}$$

Swinbank derived the sky temperature to be:

The convective heat transfer coefficient from the top cover is dependant on the wind flow over the surface of the cover. Duffie and Beckman 2013 (16) proposed the formula:

$$h_w = 2.8 + 3.0V$$

Where V is the air speed in m/s.

The radiative heat flux absorbed by the ground below the collector surface is given by:

$S = I\tau\alpha$ where I is the incident solar radiation on the collector, $\tau \; and \; \alpha$ are the transmissivity of the collector and the absorptivity of the ground.

Heat is lost to the air flow in the collector through convection as well as to the collector underneath surface through radiation. Hussain et al 2016 (26) defined the overall heat loss coefficient from ground to the ambient as given by:

$$L_d = \frac{k_g}{Z_e}$$

Whilst the radiative heat transfer between the ground and the cover underneath is given by Duffie and Beckman 2013 (16) as:

$$h_{r,g-c} = \frac{\sigma(T_g^2 + T_c^2)(T_g + T_c)}{\frac{1}{\epsilon_g} + \frac{1}{\epsilon_c} - 1}$$

The air flow within the collector is governed by the Raleigh number which is used to define whether it is laminar or turbulent. According to Hussain et al 2016 (26), the Raleigh number is calculated as:

$$R_a = Gr * Pr = \frac{g * cos\theta * \beta(T_c - T_{air}) * L_{g-c}^3}{v\alpha_c}$$

Where Gr is the Grashof number and Pr is the Prandtl number.

Heat transfer in the Solar Chimney Power plant can also be analysed using the greenhouse model. Ciprian and Bratucu 2014 (27) indicated that during the night, the internal air in the greenhouse constantly emits radiative heat. These losses can be calculated using the Walker's equation below:

$$Q_{rad} = 4.4 * 10^{-8} * S * P(T_i^4 - T_e^4)$$

Where Q_{rad} is the radiative heat loss kCal/h

S is the surface area under the cover of the greenhouse m^2

P is the transparency empirical factor. These have been determined as 0.8 for polyethylene and 0.04 for glass.

T_i and T_e are the inside and outside temperatures of the greenhouse ^oC.

Heat lost by convection is given by $Q_{conv} = k * S(T_i - T_e)$ where K is the overall heat transfer coefficient in kCal/m^2 and S is the surface area. It was noted that the convective component is higher compared to the radiative component, whilst the conduction loss component through the infrastructure and the soil has the least effect.

The heat lost to heat the incoming air through joints, cracks and broken windows in green-houses depends on the speed of the air. Ciprian and Bratucu 2014 (27) indicated that the heat gain by the incoming air is given by $Q_{inf} = 0.31 * V * (t_i - t_o)$

Heat loss through the soil depends on the convective heat transfer coefficient per Ciprian and Bratucu 2014 (27). The nature of the soil, ground water level and land moisture are some of the factors that directly influence heat loss. It is also mentioned that an increase in air speed at soil surface increases the convective heat transfer

leading to heat losses by 5-20%. This is further exacerbated if air temperatures above ground are reduced whilst the ground surface temperature are elevated.

Heat loss through evaporation can be evaluated by combining Korolkov 1955 $Q_{eva} = 0.6 * G$ and Dalton's equations $G = \eta\ (\ 21.9 + 17.8V) * (p_{ss} - p_{gp})$ where G is the amount of water evaporated in g/m^{2}h, V is the air speed, η is the coefficient equal to 0.3 and p_{ss} and p_{gp} are the water vapor pressure at soil surface as well as pressure in the vicinity of the ground.

2.3.3 The Chimney

Heat energy is converted into kinetic energy in the chimney per Zhou et al 2009 (17). This is because of the pressure difference created by the temperature difference in the chimney and the ambient. According to Al-Dabbas 2011 (28), the pressure difference between the ambient and the base of the chimney is given by:

$$\Delta P_c = g \int_0^{Hc} (\rho_\infty - \rho) dh \qquad \ldots\ldots\ldots \qquad (10)$$

Where H_c is the height of the chimney, ρ is the density of air along the height of the chimney and ρ_∞ is the density of ambient air.

Al-Dabbas 2011 (28) summarised the change in pressure as:

$$\Delta P_c = 0.00353 g H [\frac{\Pi G \eta_{coll}}{C_p \dot{m}} R_{coll}^2 - \frac{g}{2C_p} H + \frac{1}{2} \gamma_4 H \qquad \ldots\ldots \qquad (11)$$

Where γ_4 is the temperature lapse rate.

Pretorius 2004 (29) indicated that the generated power of the turbine is related to the pressure drop across the turbine which is calculated using the formula:

$$\Delta P_{turb} = \Delta P - (\Delta P_i + \Delta P_{coll} + \Delta P_{turb,i} + \Delta P_t + \Delta P_{to} + \Delta P_{dyn}) \quad \ldots\ldots (12)$$

where ΔP is the driving potential, ΔP_i the collector inlet pressure drop and ΔP_{coll} is the total pressure drop through the collector, $\Delta P_{turb,i}$ is the turbine inlet pressure drop, ΔP_t is the total pressure drop through the tower, ΔP_{to} is the tower outlet pressure differential and ΔP_{dyn} is the tower dynamic outlet loss.

Chitsomboon and Koonsrisuk 2012 (32) concluded that pressure difference between the air inside the chimney and the ambient air gives the driving pressure. Assuming frictional losses to be negligible, part of the driving pressure is used to drive the turbine and the other is consumed as the kinetic energy of the airflow.

$$\Delta P A_c V_2 = \frac{q" A_r g h_c \beta}{C_p} \qquad \text{……..} \qquad (13)$$

Where A_r is the area of the collector.

A convective and ventilation transfers in greenhouses by Roy et al 2002 (31) defined the chimney effect to be approximated by the Boussinesq approximation. When both wind and buoyancy forces are considered for ventilation on a greenhouse with roof and side openings, the wind follow rate is given by:

$$Q = C_d(2g\frac{\Delta T}{T}\left(\frac{(A_r A_s)^2}{A_r^2 + A_s^2}\right) + (\frac{A_r + A_s}{2})^2 C_w u^2)^{0.5}$$

Where $A_r \; and \; A_s$ are the roof and side opening areas, $C_d \; and \; C_w$ area the wind effect and discharge coefficients respectively.

Al-Dabbas 2011 (28) indicated that the maximum chimney height was given as:

$$H_{max} = \frac{C_p \dot{m}}{U \Pi D} \ln[\frac{\Pi^2 UDG \eta_{coll} R^2}{C_p m^2 (g - C_p Y_4)} + 1] \qquad \text{……..} \qquad (14)$$

2.3.2 The turbine

According to Thakre et al 2013 (14), the available power in the wind as it enters the chimney is given by:

$$Power = \sqrt{\frac{2(\frac{gh_o\Delta T_i)^3}{(T_a A_i^3)}}{A_c^2(T_a+\Delta T_i)}} \qquad \text{……..} \qquad (15)$$

Where A_i is the entrance area of the chimney, h_o is the height of the chimney entrance above ground and T_a is the ambient temperature.

Zhou 2009 (17) derived the work done by the air at the turbine as:

$$\Delta P_t A_c U_{in} = \dot{m} C_p (T_{in} - T_{out}) + \frac{1}{2}\dot{m}(U_{in}^2 - U_{out}^2) + \dot{m}g\big(0 - (H + l\sin\alpha)\big) -$$

$$U(\bar{T} - \overline{T_{m\infty}})\Pi D(H + l) \qquad \text{…….} \qquad (16)$$

Where $\bar{T} = T_{in} - \frac{\Delta T_c}{2}$, U is the overall heat transfer coefficient.

Koonsrisuk and Chitsomboon (32) simplified the pressure equations before and after the turbine. The pressure before the turbine is expressed as:

$$P_2 = P_a + \frac{\dot{m}q"}{2\Pi\rho_a C_p T_a h_r^2}\ln\frac{r_r}{r_c} - \frac{\dot{m}^2}{2\rho_1}\left(\frac{1}{A_2^2} - \frac{1}{A_1^2}\right) \qquad \text{…….} \qquad (17)$$

where P_a, ρ_a, T_a are the pressure, density and temperature of ambient air, r_r, r_c is radius of collector and chimney respectively and h_r is the height of the collector from ground.

Power generated by the wind turbine Zhou et al 2009 (17) can be calculated as:

$$P_{out} = \eta_{turb}\Delta P_{turb} A_c U_{in} \qquad \text{…….} \qquad (18)$$

Where η_{turb} is the efficiency of the turbine and generator system,

An analysis of turbine rotor diameters for capacity between 20kW to 30kW in 2016 (34) has been summarised in the table below. This will enable to determine the diameter of the chimney:

Table 2:25kW turbines on the market

	Manufacturer	Turbine name & blades	Rated Power (kW)	Cut-in speed (m/s)	Rated speed (m/s)	Cut-out speed (m/s)	Rotor Diameter (m)	Life time (years)
1	Eoltec	Wind runner/2 blades	25	3	12	None	10	25
2	Eurowind Small turbines Ltd	Eurowind 19kW/ 3blades	19	3-4	12	28-32	8.25	20
3	Eurowind Small turbines Ltd	Eurowind 30kW/ 3blades	30	3-4	12	28-32	10.25	20
4	Fuhrlander	FL30 / 3 blades	30	2.5	12	25	13	25
5	Pitchwind Systems AB	Pitchwind 20-30kW/2 blades	20-30	2	15	None	14	20
6	Solid Wind Power	SWP 25-14TG20 /3 blades	24.5-28.6	3	12.5	25	14	20

It is evident that the minimum and maximum rotor diameters from the above table are 8.25 and 14 metres respectively. Thus, a turbine chimney diameter of 14 metres will be used in the model.

Chapter 3: Methodology

3.1 Introduction

The study involves identifying existing works carried out on the SCCP technology and develop a mathematical model than can be used in Zimbabwe to design SCPP. This entails developing mathematical models for the solar collector, chimney, wind turbine and wind flow within the chimney.

For the solar collector, an analysis of a single cover air heater made of glass or plastic and the ground as the back plate will be evaluated in terms of radiative and convective heat transfer as well as the overall loss coefficient, the overall temperature gain within the collector and the heat transfer to the air mass and finally the air movement.

The optimum chimney height, diameter and optimum position of the turbine within the chimney will be determined. Pressure variations in the chimney are critical to establish air movement and eventually energy output.

The mathematical model will be used to simulate exist prototype plants as well as validate results obtained by previous researchers.

The turbine will then be assessed its performance under four scenarios as follows;

iv. The capacity factor of the turbine.
v. The total energy generated annually.
vi. Ability to supply an off-grid community with a defined load profile. The load profile will be extrapolated from the national demand profile.

Additional assessment criteria will be the cost and size of battery storage capacity that needs to be installed for a continuous power supply.

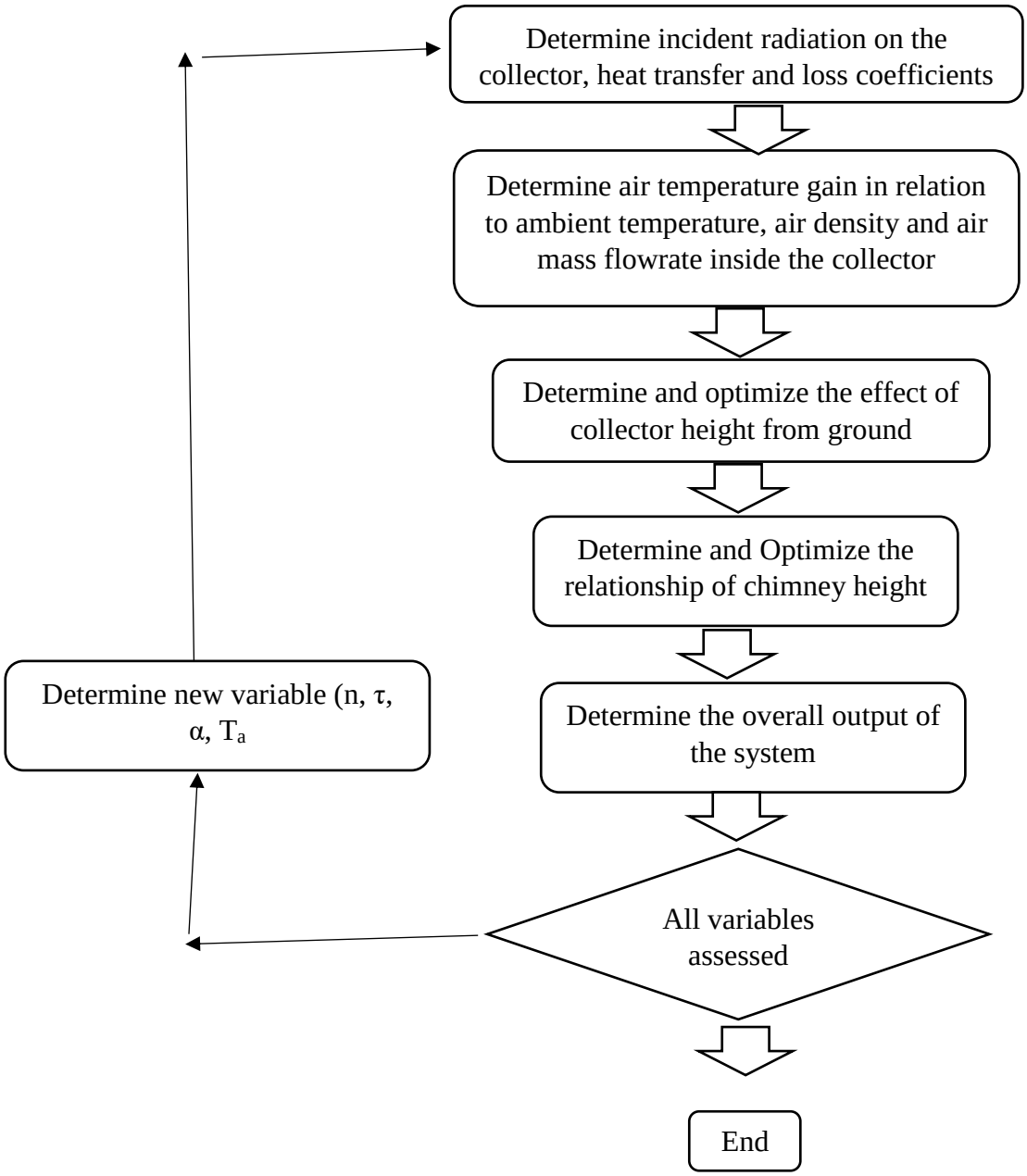

Three areas of Kariba, Gweru and Harare have been selected for analysis based on the following reasons:

i. Varying weather conditions, Gweru is known to be the coldest place in Zimbabwe, whilst Harare is moderate and Kariba is rated one of the hottest places in the country.

ii. Availability of data from the meteorological centres as weather stations are located in these places.

iii. Varying wind patterns.

3.2 Incident radiation on the collector

The solar chimney technology is dependent on the solar radiation incident on the collector. It therefore follows that the number of daylight hours for a place have a bearing on the performance of the plant. Duffie and Beckman 2013 (16) showed that the monthly average extra-terrestrial radiation on a surface is given by:

$$\overline{H_o} = \frac{24*3600G_{sc}}{\Pi}\left(1 + 0.033\cos\frac{360n}{365} * \left(\cos\Phi\cos\delta\cos w_s + \frac{\Pi w_s}{180}\sin\Phi\sin\delta\right)\right)$$

……. (1)

Where Φ is the latitude, n is the day number and δ is the declination angle is given by:

$$\delta = \frac{180}{\Pi}(0.006918 - 0.399912\cos B + 0.07020257\sin B - 0.006758\cos 2B +$$

$$0.000907\sin 2B - 0.002697\cos 3B + 0.00148\sin 3B \quad \ldots\ldots. \quad (2)$$

Where $B = (n-1)\frac{2\Pi}{365}$ ……. (3)

And $w_s\ is\ the\ sunset\ hour\ angle = -\tan\Phi\tan\delta$ ……. (4)

Using the monthly average solar radiation measured at Harare, Gweru and Kariba, the incident solar radiation on the collector was determined through the following steps:

3.3 Solar plate collector

Using the analysis of air heaters Duffie and Beckman 2013 (16) as shown below.

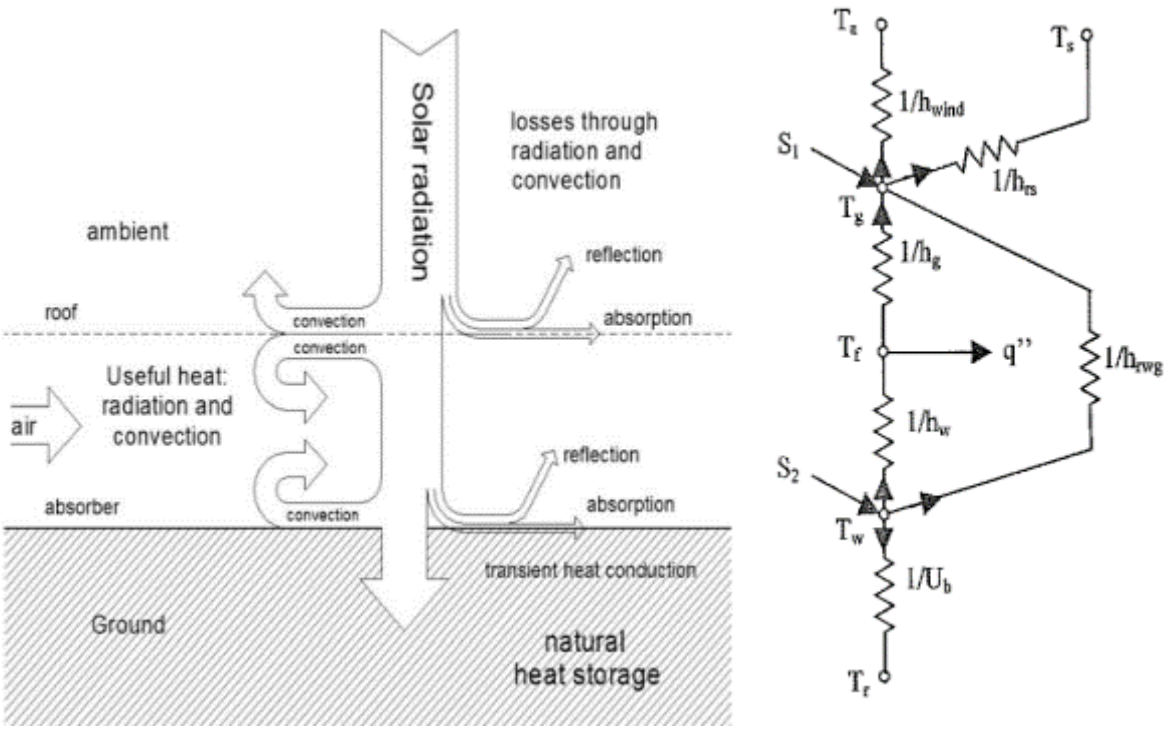

Figure 5:Solar air heater thermal network (Bernades, Backstrom and Ong)

It is postulated that incident solar radiation ($S_2 = S_1\alpha\tau$) is absorbed heats up the ground to a temperature T_p. Part of the energy is stored by the ground increasing ground temperature whilst part of the energy is transferred to the inlet air through convection heat transfer coefficient, h_2. Through radiation, heat is transferred to the collector cover through the radiative heat transfer coefficient h_r. Heat is also transferred between the air and the collector cover through convection, h_1 and to the ambient through radiation and convection U_t.

The energy balance equations for the collector cover, the ground and the air flow Duffie and Beckman 2013 (16) and Ong 2002 (19) can be given by:

$$T_c: S_1 + h_r(T_p - T_c) + h_1(T_f - T_c) = U_t(T_c - T_a)$$

$$T_p: S_2 = h_2(T_p - T_f) + h_r(T_p - T_c) + U_b(T_p - T_{ps})$$

$$T_f: h_2(T_p - T_f) = h_1(T_f - T_c) + \dot{q}"$$

The overall heat transfer coefficient from the collector cover to the ambient is given by Duffie and Beckman 2013 (16):

$$U_t = \left(\frac{1}{h_{c,p-c}+h_{r,p-c}} + \frac{1}{h_w+h_{r,c-a}}\right)^{-1} \quad \ldots\ldots\ldots \quad (19)$$

Where the radiation coefficient $h_{r,g-c}$, from the ground to the cover is given by:

$$h_{r,g-c} = \frac{\sigma(T_g^2+T_c^2)(T_g-T_c)}{\frac{1}{\epsilon_g}+\frac{1}{\epsilon_c}-1} \quad \ldots\ldots\ldots \quad (20)$$

And $h_{r,c-a}$ is given by

$$h_{r,c-a} = \epsilon_c \sigma (T_c^2 + T_s^2)(T_c - T_s) \quad \ldots\ldots\ldots \quad (21)$$

And the collector cover temperature will be calculated using the equation:

$$T_c = T_g - \frac{U_t(T_g-T_a)}{h_{c,g-c}+h_{r,g-c}} \quad \ldots\ldots\ldots \quad (22)$$

The volumetric air flow rate from the collector will be determined by Ong 2002 (19):

$$\dot{V}_o = C_d * \frac{A_o}{\sqrt{(1+A_r)}} * \sqrt{\frac{2gL(T_f-T_r)}{T_r}}$$

Where T_f, T_r are the temperature for the air flow and room temperature.

Thus the air mass flow rate can be derived as

$$\dot{m} = C_d * \frac{\rho_{f,o} A_o}{\sqrt{(1+A_r)}} * \sqrt{\frac{2gL(T_f-T_r)}{T_r}}$$

It is assumed that the air movement between the ground and the collector is laminar ($R_a < 10^9$) and hence the Nusselt number will be given by:

$$Nu = 0.68 + \left(\frac{0.67{R_a}^{0.25}}{\left[1 + \left(0.492/P_r\right)^{\frac{9}{16}}\right]^{\frac{4}{9}}}\right)$$

The overall heat loss coefficients U_L for the solar chimney power plant can be accounted for by two broad categories from the top of the collector cover and absorption by the ground. The

absence of edges on the collector to allow for free air movement simplifies the calculation of the overall collector heat loss coefficients to:

$$U_L = U_t + U_g$$

Where U_t and U_g are the top cover loss coefficient and the ground surface.

The radiative heat transfer between the ground and the glass cover was derived to be :

$$h_{rgc} = \frac{\sigma(T_c^2 + T_g^2)(T_c + T_g)}{(\frac{1}{\epsilon_c} + \frac{1}{\epsilon_g} - 1)}$$

And the convective heat transfer from the collector due to wind is given by:

$$h_{cw} = 5.7 + 3.8V$$

3.4 Turbine

From equation 2.3.4.4 the change in pressure can be calculated after elimination of the sloped part of the chimney. It is assumed that the solar power plant will utilize a vertical chimney that does not use mountains. The pressure equation is therefore stated as:

$$\Delta P_t A_c U_{in} = \dot{m} C_p (T_{in} - T_{out}) + \frac{1}{2}\dot{m}(U_{in}^2 - U_{out}^2) + \dot{m} g H - U(\bar{T}) \Pi D H \quad \ldots(23)$$

Where $\bar{T} = T_{in} - \frac{\Delta T_c}{2}$, U is the convective heat transfer coefficient between the chimney wall and the inside airflow.

The change in air flows temperature between the inlet and the outlet of the chimney can be derived from Zhou et al 2009 (17) by eliminating the temperature of the mountain. The following formula can be used:

$$\Delta T_{ch} = \frac{\dot{m} g H + \Delta P_t A_{ch} U_{in} - \frac{1}{2} m (U_{in}^2 - U_{out}^2) + \dot{U} \Pi D H (T_a + \Delta T_c)}{2 C_p \dot{m} + \frac{1}{2} U \Pi D H} \quad \ldots\ldots\ldots \quad (24)$$

The change in pressure within the chimney can be derived using the equation:

$$\Delta P_{ch} = \beta \rho g H\left(\Delta T_c + \frac{\dot{m}H + (C_p r_\infty - g) + \Delta P_t A_{ch} U_{in} - \frac{1}{2}\dot{m}\left(U_{in}^2 - U_{out}^2\right) + U\dot{\Pi} DH\left(\frac{r_\infty H}{2} - T_a - \Delta T_c\right)}{2C_p\dot{m} + \frac{1}{2}U\Pi DH}\right) \quad \text{.....(25)}$$

Where β is the expansion coefficient of air, ρ is the density of air

Chapter 4: Data Collection

4.1 Introduction

The analysis of solar chimney power plants in Zimbabwe involves analysis of solar radiation data across the country. Based on earlier works by Hove and Gottsche 1999 (10) were global solar radiation over Zimbabwe was mapped using data from thirty (30) meteorological stations.

Table 3:Meteo Station data used in the analysis (Source Hove et al)

BEITBRIDGE	MATOPOS	CHISUMBANJE
BINGA	MOUNT DARWIN	HWANGE
BULAWAYO	MUKANDI	CHISENGU
GWERU	NYANGA	CHIPINGE
HARARE	HENDERSON	BANKET
KADOMA	RUSAPE	CHIVHU
KARIBA	BUFFALO RANGE	GOKWE
KAROI	TSHOLOTSHO	KWEKWE
MARONDERA	VICTORIA FALLS	GRAND REEF
MASVINGO	WEST NICHOLSON	MAKOHOLI

The data was extrapolated to map the solar radiation over Zimbabwe to refine the map from the one shown below;

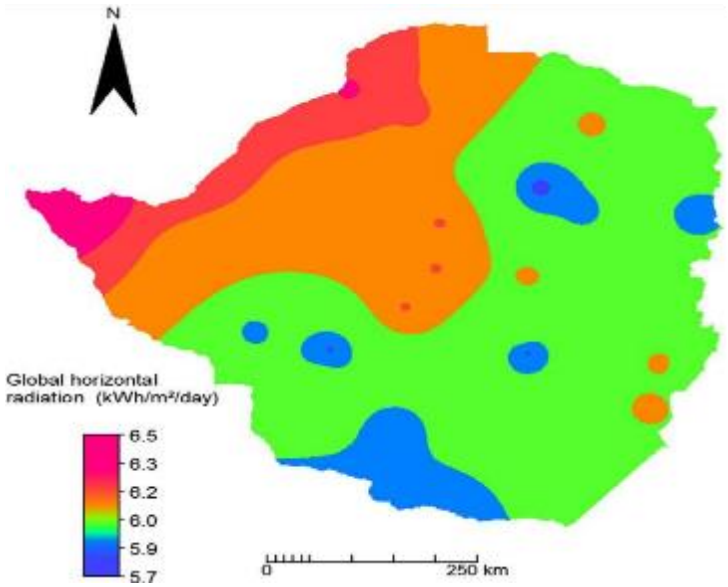

Figure 6:Solar radiation map for Zimbabwe (source -researchgate)

Through the interpolation, it is possible to predict the solar radiation of any point in Zimbabwe within 50km radius.

4.2 Analysis of solar radiation at Harare, Gweru and Kariba

Using the data obtained from the weather stations above, it was predicted that the radiation at the three selected sites of Harare(latitude -17.8 and longitude 31.1, Kariba (latitude -16.5 and longitude 28.9 and Gweru (latitude -19.45 and longitude 29.1) would vary as shown in tables 7, 8, 9 and 10 below using the Hove and Gottsche and the Collares-Perreira-Rabl models.

Table 4:Incident radiation at Harare (W/m2) based on Collares-Perreira-Rabl model

Hour ending	Jan	Feb	Mar	Apr	May	Jun	Jul	Aug	Sep	Oct	Nov	Dec
6	0.00	0.00	0.00	0.00	0.00	0.00	0.00	0.00	0.00	0.00	0.00	2.35
7	106.40	91.05	76.28	64.95	55.66	0.00	52.73	68.07	78.89	90.28	101.70	109.39
8	251.62	242.85	249.39	248.95	236.72	226.15	230.85	260.85	274.87	280.09	263.98	251.33
9	408.70	408.75	440.75	454.99	441.81	426.82	433.37	477.79	492.57	488.17	440.01	404.49
10	555.82	565.10	622.33	652.01	639.26	620.68	628.74	685.83	699.77	684.64	605.14	547.71
11	670.07	686.99	764.49	806.95	795.15	774.05	783.17	849.72	862.26	837.99	733.51	658.83
12	732.54	753.78	842.55	892.23	881.13	858.74	868.42	940.01	951.57	922.05	803.74	719.56
13	732.54	753.78	842.55	892.23	881.13	858.74	868.42	940.01	951.57	922.05	803.74	719.56
14	670.07	686.99	764.49	806.95	795.15	774.05	783.17	849.72	862.26	837.99	733.51	658.83
15	555.82	565.10	622.33	652.01	639.26	620.68	628.74	685.83	699.77	684.64	605.14	547.71
16	408.70	408.75	440.75	454.99	441.81	426.82	433.37	477.79	492.57	488.17	440.01	404.49
17	251.62	242.85	249.39	248.95	236.72	226.15	230.85	260.85	274.87	280.09	263.98	251.33
18	106.40	91.05	76.28	64.95	55.66	0.00	52.73	68.07	78.89	90.28	101.70	109.39
19	0.00	0.00	0.00	0.00	0.00	0.00	0.00	0.00	0.00	0.00	0.00	2.35
Tilt factor	0.941	0.97	1.015	1.104	1.204	1.24	1.241	1.161	1.059	0.976	0.937	0.935
K_T	0.508	0.516	0.583	0.64	0.668	0.677	0.676	0.692	0.670	0.640	0.561	0.503

Table 5:Incident radiation at Harare (W/m2) based on Hove & Gottsche model

Hour ending	Jan	Feb	Mar	Apr	May	Jun	Jul	Aug	Sep	Oct	Nov	Dec
6	0.00	0.00	0.00	0.00	0.00	0.00	0.00	0.00	0.00	0.00	0.00	1.78
7	92.84	83.29	75.75	67.58	59.35	0.00	56.67	70.67	79.70	88.36	92.73	94.35
8	239.12	236.16	249.59	251.99	240.71	230.64	235.07	263.73	276.00	278.60	255.84	237.35
9	397.16	403.01	441.61	458.40	446.08	431.56	437.84	480.92	493.99	487.06	432.61	391.46
10	545.05	560.15	623.74	655.73	643.74	625.62	633.41	689.18	701.42	683.85	598.35	535.46
11	659.85	682.59	766.27	810.88	799.79	779.14	787.99	853.21	864.07	837.41	727.15	647.14
12	722.60	749.66	844.53	896.27	885.85	863.90	873.31	943.58	953.47	921.59	797.61	708.15
13	722.60	749.66	844.53	896.27	885.85	863.90	873.31	943.58	953.47	921.59	797.61	708.15
14	659.85	682.59	766.27	810.88	799.79	779.14	787.99	853.21	864.07	837.41	727.15	647.14
15	545.05	560.15	623.74	655.73	643.74	625.62	633.41	689.18	701.42	683.85	598.35	535.46
16	397.16	403.01	441.61	458.40	446.08	431.56	437.84	480.92	493.99	487.06	432.61	391.46
17	239.12	236.16	249.59	251.99	240.71	230.64	235.07	263.73	276.00	278.60	255.84	237.35
18	92.84	83.29	75.75	67.58	59.35	0.00	56.67	70.67	79.70	88.36	92.73	94.35
19	0.00	0.00	0.00	0.00	0.00	0.00	0.00	0.00	0.00	0.00	0.00	1.78
Tilt factor	0.917	0.958	1.016	1.111	1.214	1.25	1.252	1.168	1.062	0.975	0.923	0.908

K_T	0.508	0.516	0.583	0.64	0.668	0.677	0.676	0.692	0.67	0.64	0.561	0.503

Table 6:Incident radiation at Kariba (W/m2) based on Collares- Perreira-Rabl model

Hour ending	Jan	Feb	Mar	Apr	May	Jun	Jul	Aug	Sep	Oct	Nov	Dec
6	0.00	0.00	0.00	0.00	0.00	0.00	0.00	0.00	0.00	0.00	0.00	0.00
7	103.16	93.39	79.40	75.66	74.66	62.18	67.55	77.02	82.45	92.15	98.51	103.67
8	264.87	273.60	261.47	274.39	279.40	249.21	261.27	281.30	284.73	294.39	283.12	275.38
9	439.92	470.38	462.54	496.41	510.49	461.52	480.67	510.60	509.18	516.07	483.43	460.73
10	603.93	655.75	653.23	708.42	732.49	666.16	691.87	730.18	722.67	725.38	671.36	634.09
11	731.35	800.21	802.47	875.01	907.55	827.84	858.60	903.01	890.02	888.73	817.49	768.62
12	801.02	879.36	884.40	966.67	1004.05	917.06	950.56	998.18	981.98	978.29	897.44	842.14
13	801.02	879.36	884.40	966.67	1004.05	917.06	950.56	998.18	981.98	978.29	897.44	842.14
14	731.35	800.21	802.47	875.01	907.55	827.84	858.60	903.01	890.02	888.73	817.49	768.62
15	603.93	655.75	653.23	708.42	732.49	666.16	691.87	730.18	722.67	725.38	671.36	634.09
16	439.92	470.38	462.54	496.41	510.49	461.52	480.67	510.60	509.18	516.07	483.43	460.73
17	264.87	273.60	261.47	274.39	279.40	249.21	261.27	281.30	284.73	294.39	283.12	275.38
18	103.16	93.39	79.40	75.66	74.66	62.18	67.55	77.02	82.45	92.15	98.51	103.67
19	0.00	0.00	0.00	0.00	0.00	0.00	0.00	0.00	0.00	0.00	0.00	0.00
Tilt factor	0.925	0.954	1.012	1.102	1.204	1.250	1.233	1.151	1.053	0.972	0.92	0.903
K_T	0.562	0.606	0.609	0.686	0.750	0.713	0.730	0.729	0.688	0.678	0.633	0.602

Table 7: Incident solar radiation W/m2 H&G Kariba

Hour ending	Jan	Feb	Mar	Apr	May	Jun	Jul	Aug	Sep	Oct	Nov	Dec
6	0.00	0.00	0.00	0.00	0.00	0.00	0.00	0.00	0.00	0.00	0.00	0.00
7	93.33	89.28	78.98	77.38	81.00	66.50	72.55	80.40	83.14	90.84	93.99	95.83
8	255.71	269.99	261.52	276.36	286.19	253.78	266.58	285.01	285.66	293.33	278.97	268.03
9	431.37	467.21	463.02	498.59	517.69	466.31	486.27	514.61	510.34	515.24	479.60	453.83
10	595.88	652.94	654.07	710.78	740.03	671.14	697.69	734.43	724.00	724.73	667.81	627.54
11	723.65	797.66	803.56	877.49	915.32	832.95	864.58	907.42	891.48	888.22	814.13	762.32
12	793.50	876.94	885.62	969.21	1011.94	922.23	956.63	1002.68	983.50	977.85	894.17	835.97
13	793.50	876.94	885.62	969.21	1011.94	922.23	956.63	1002.68	983.50	977.85	894.17	835.97
14	723.65	797.66	803.56	877.49	915.32	832.95	864.58	907.42	891.48	888.22	814.13	762.32
15	595.88	652.94	654.07	710.78	740.03	671.14	697.69	734.43	724.00	724.73	667.81	627.54
16	431.37	467.21	463.02	498.59	517.69	466.31	486.27	514.61	510.34	515.24	479.60	453.83
17	255.71	269.99	261.52	276.36	286.19	253.78	266.58	285.01	285.66	293.33	278.97	268.03
18	93.33	89.28	78.98	77.38	81.00	66.50	72.55	80.40	83.14	90.84	93.99	95.83
19	0.00	0.00	0.00	0.00	0.00	0.00	0.00	0.00	0.00	0.00	0.00	0.00
Tilt factor	0.909	0.949	1.013	1.107	1.219	1.262	1.246	1.159	1.055	0.971	0.913	0.891
K_T	0.562	0.606	0.609	0.686	0.750	0.713	0.730	0.729	0.688	0.678	0.633	0.602

Table 8:Incident solar radiation W/m2 Gweru- Collares-pereire-Rabl

Hour ending	Jan	Feb	Mar	Apr	May	Jun	Jul	Aug	Sep	Oct	Nov	Dec
6	1.56	0.00	0.00	0.00	0.00	0.00	0.00	0.00	0.00	0.00	0.00	6.43
7	109.46	96.33	79.94	64.48	60.68	0.00	0.00	74.58	85.95	92.66	104.06	113.06
8	273.85	270.58	262.26	249.52	250.02	239.45	249.10	280.05	297.21	289.12	277.21	266.94
9	451.18	460.62	463.78	457.08	465.05	450.13	464.81	511.69	531.94	504.32	464.65	432.58
10	616.97	639.50	655.00	655.76	672.37	654.05	673.25	734.07	755.38	707.42	640.26	587.22
11	745.60	778.85	804.69	812.09	836.18	815.54	838.18	909.36	930.63	865.89	776.68	707.09
12	815.88	855.16	886.89	898.18	926.59	904.77	929.25	1005.97	1026.95	952.75	851.28	772.57
13	815.88	855.16	886.89	898.18	926.59	904.77	929.25	1005.97	1026.95	952.75	851.28	772.57
14	745.60	778.85	804.69	812.09	836.18	815.54	838.18	909.36	930.63	865.89	776.68	707.09
15	616.97	639.50	655.00	655.76	672.37	654.05	673.25	734.07	755.38	707.42	640.26	587.22
16	451.18	460.62	463.78	457.08	465.05	450.13	464.81	511.69	531.94	504.32	464.65	432.58

17	273.85	270.58	262.26	249.52	250.02	239.45	249.10	280.05	297.21	289.12	277.21	266.94
18	109.46	96.33	79.94	64.48	60.68	0.00	0.00	74.58	85.95	92.66	104.06	113.06
19	1.56	0.00	0.00	0.00	0.00	0.00	0.00	0.00	0.00	0.00	0.00	6.43
Tilt factor	0.917	0.957	1.021	1.118	1.242	1.282	1.262	1.190	1,074	0.977	0.925	0.918
K_T	0.572	0.589	0.614	0.646	0.701	0.711	0.720	0.739	0.722	0.662	0.597	0.544

Table 9:Incident radiation at Gweru (W/m2) based on Hove & Gottsche model

Hour ending	Jan	Feb	Mar	Apr	May	Jun	Jul	Aug	Sep	Oct	Nov	Dec
6	1.26	0.00	0.00	0.00	0.00	0.00	0.00	0.00	0.00	0.00	0.00	5.05
7	99.18	91.04	79.54	67.12	64.41	0.00	0.00	79.18	86.98	91.04	96.87	99.69
8	264.47	266.11	262.53	252.62	254.09	244.61	254.49	285.20	298.67	287.91	270.76	254.63
9	442.62	456.88	464.65	460.60	469.42	455.60	470.55	517.33	533.80	503.47	458.87	421.21
10	609.07	636.36	656.35	659.61	676.99	659.77	679.28	740.12	757.57	706.87	635.02	576.63
11	738.16	776.13	806.38	816.19	840.98	821.45	844.40	915.70	933.04	865.55	771.83	697.05
12	808.68	852.67	888.75	902.39	931.47	910.77	935.58	1012.46	1029.48	952.52	846.63	762.81
13	808.68	852.67	888.75	902.39	931.47	910.77	935.58	1012.46	1029.48	952.52	846.63	762.81
14	738.16	776.13	806.38	816.19	840.98	821.45	844.40	915.70	933.04	865.55	771.83	697.05
15	609.07	636.36	656.35	659.61	676.99	659.77	679.28	740.12	757.57	706.87	635.02	576.63
16	442.62	456.88	464.65	460.60	469.42	455.60	470.55	517.33	533.80	503.47	458.87	421.21
17	264.47	266.11	262.53	252.62	254.09	244.61	254.49	285.20	298.67	287.91	270.76	254.63
18	99.18	91.04	79.54	67.12	64.41	0.00	0.00	79.18	86.98	91.04	96.87	99.69
19	1.26	0.00	0.00	0.00	0.00	0.00	0.00	0.00	0.00	0.00	0.00	5.05
Tilt factor	0.902	0.95	1.022	1.126	1.252	1.294	1.274	1.202	1.077	0.976	0.915	0.896
K_T	0.572	0.589	0.614	0.646	0.701	0.711	0.720	0.739	0.722	0.662	0.597	0.544

4.3 Sample Test data in Spain

The research analysis also used data on the existing Solar chimney power plant in Spain.

Schlaich et al 1997 (7) worked extensively on the project and from the publications it was noted that the Manzanares project as the following parameters.

Table 10:Manzanares prototype dimensions and technical data (Source Schlaich et al)

Tower height	194.6m
Tower radius	5.08m
Mean collector radius	122.0m
Mean roof height	1.85m
Number of turbine blades	4
Turbine blade profile	FX W-151-A
Blade tip speed to air transport velocity ratio	1:10
Typical air temperature increase	$\Delta T = 20k$
Nominal output	50kW
Collector covered with plastic	40,000 m^2
Collector covered with glass	6,000 m^2

Chapter 5: Mathematical Modelling

5.1 Introduction

The research involved developing a mathematical model that can predict the electrical output of a solar chimney power plant in Zimbabwe. Using this model the output of the Manzanares prototype using the dimensions and technical data in Chapter 4 was used to ascertain the correctness of the model.

The mathematical model inputs include and were limited to the following;

1. The geographical coordinates of the place

   The model operates based on the latitude and longitude of the specified area. The coordinates are referenced to the 50km grid points were data exists on the global solar radiation.

   Latitudes coordinates can vary between -16.5 to -22.5 whilst longitudinal coordinates vary between 25.5 and 33 degrees.

   Based on the latitude of the area, the collector optimised tilt is latitude + 5º.

2. The collector parameters

   Regarding the Manzanares dimensions data, the inputs to the model were restricted to the chimney height, chimney radius, collector radius and the height of the collector above ground.

   The basic collector material parameters which include emittance of the cover material, the transmittance and absorptance of the cover material are critical in determining the convective and radiative transfer coefficients of the plant.

The emittance of the ground was estimated based on publications from Jin and Liang 2006 (35) that established the emittance of ground to be 0.9.

3. Other importance parameters that need to be defined include the maximum and minimum temperatures for the area, the azimuth of the collector was set at 180 degrees (North facing). Various soil types can be chosen from the list provided. Appendix 1 shows the various soil types that are found in Zimbabwe as well as the thermal parameters used in the analysis.

5.2 Incident radiation on an area

5.2.1 Declination angle

The declination angle for the chosen place was calculated using the empirical formula by Spencer as: $\delta = \frac{180}{\Pi} * 0.006918 - 0.399912cosB + 0.070257SinB - 0.002697cos3B + 0.00148Sin3B$

Where $B = (n-1) * \frac{2\Pi}{365}$

The mathematical model uses the average day of the month to compute the declination angle. The average day for the month are defined by Duffie and Beckman 2013 (16) as shown below:

Table 11: Average day for each month (Duffie and Beckman)

Month	Date	Average day n
January	17	17
February	16	47
March	16	75
April	15	105
May	15	135
June	11	162
July	17	198
August	16	228
September	15	258
October	15	288

November	14	318
December	10	344

5.1.2 Hour angle (W_s)

The hour angle (W_s) which defines the displacement of the sun east or west of the local meridian with each hour traversing 15°, was used to determine when the sun rises and sets.

$$W_s = cos^{-1}(tan\Phi * \tan\delta)$$

As defined by Duffie and Beckman (16) morning hours give negative W_s whilst afternoon periods are positive.

5.2.2 Extra-terrestrial radiation (H_o)

In order to calculate the clearness index for the areas specified, it is critical to establish the extra-terrestrial radiation that would be incident on the area. Two equations that yielded the same results were used to ascertain the computations.

$$H_o = \left(\frac{24 * 3600 * 1367}{\Pi}\right) * (1 + 0.033\cos\left(\frac{2\Pi n}{365}\right) cos\Phi cos\delta sinW_s + \frac{\Pi W_s}{180} * Sin\Phi Sin\delta)$$

The global monthly solar radiation (H) for the area is extrapolated from the existing measured data from the 30 stations mentioned in Chapter 4.

The clearness index is the n computed as the ratio of the global solar radiation (H) measured at ground level to the extra-terrestrial radiation that is incident on the area.

$$k_T = \frac{H}{H_o}$$

5.2.3 Diffuse Fraction

The diffuse fraction defined as the fraction of the radiation incident on an area because of scattering to the total radiation incident on that area was calculated based on the Hove and Gottsche correlation (10) based on Zimbabwean data;

$\frac{\bar{H}_d}{\bar{H}_h} = 1.0294 - 1.144k_T$ for 0.47< k_T < 0.75

$\frac{\bar{H}_d}{\bar{H}_h} = 0.175$ for k_T > 0.175

This was compared by using the Collares-Pereira-Rabl correlation (16) defined below.

$\frac{H_d}{H} = 0.99 \quad for\ k_T \leq 0.17$

$\frac{H_d}{H} = 1.188 - 2.272k_T + 9.473k_T^2 - 21.865k_T^3 + 14.648k_T^4 \quad for\ 0.17 < k_T < 0.75$

$\frac{H_d}{H} = -0.54k_T + 0.632 \quad for\ 0.75 < k_T < 0.8$

$\frac{H_d}{H} = 0.2 \quad for\ k_T \geq 0.80$

Despite the above models giving the same results during most months and hours, huge variations were noted during the months of December and January and morning hours.

Table 12:Tilt factor variations between Hove & Gottsche against Collares-Pereira-Rabl model

Hour ending	Jan	Feb	Mar	Apr	May	Jun	Jul	Aug	Sep	Oct	Nov	Dec
6	0.00%	0.00%	0.00%	0.00%	0.00%	0.00%	0.00%	0.00%	0.00%	0.00%	0.00%	32.02%
7	14.61%	9.32%	0.70%	-3.89%	-6.22%	0.00%	-6.95%	-3.68%	-1.02%	2.17%	9.67%	15.94%
8	5.23%	2.83%	-0.08%	-1.21%	-1.66%	-1.95%	-1.80%	-1.09%	-0.41%	0.53%	3.18%	5.89%
9	2.91%	1.42%	-0.19%	-0.74%	-0.96%	-1.10%	-1.02%	-0.65%	-0.29%	0.23%	1.71%	3.33%
10	1.98%	0.88%	-0.23%	-0.57%	-0.70%	-0.79%	-0.74%	-0.49%	-0.24%	0.12%	1.13%	2.29%
11	1.55%	0.64%	-0.23%	-0.48%	-0.58%	-0.65%	-0.61%	-0.41%	-0.21%	0.07%	0.87%	1.81%
12	1.38%	0.55%	-0.23%	-0.45%	-0.53%	-0.60%	-0.56%	-0.38%	-0.20%	0.05%	0.77%	1.61%
13	1.38%	0.55%	-0.23%	-0.45%	-0.53%	-0.60%	-0.56%	-0.38%	-0.20%	0.05%	0.77%	1.61%
14	1.55%	0.64%	-0.23%	-0.48%	-0.58%	-0.65%	-0.61%	-0.41%	-0.21%	0.07%	0.87%	1.81%
15	1.98%	0.88%	-0.23%	-0.57%	-0.70%	-0.79%	-0.74%	-0.49%	-0.24%	0.12%	1.13%	2.29%
16	2.91%	1.42%	-0.19%	-0.74%	-0.96%	-1.10%	-1.02%	-0.65%	-0.29%	0.23%	1.71%	3.33%
17	5.23%	2.83%	-0.08%	-1.21%	-1.66%	-1.95%	-1.80%	-1.09%	-0.41%	0.53%	3.18%	5.89%
18	14.61%	9.32%	0.70%	-3.89%	-6.22%	0.00%	-6.95%	-3.68%	-1.02%	2.17%	9.67%	15.94%
19	0.00%	0.00%	0.00%	0.00%	0.00%	0.00%	0.00%	0.00%	0.00%	0.00%	0.00%	32.02%

Based on the huge variations in the incident radiation on a tilted plane from the two models, it was resolved to use the Hove and Gottsche model in the study. This is because the Hove and Gottsche model was derived based on Zimbabwe data and hence gives a realistic view of radiation in Zimbabwe.

5.2.4 Hourly diffuse and total radiation

With the diffuse fraction calculated, the daily diffuse radiation was calculated based on the Liu and Jordan (1960) formula;

$$r_d = \frac{\Pi}{24}\frac{(cosW - \cos W_s)}{\sin W_s - \frac{\pi W_s}{180}\cos W_s}$$

And the total radiation was calculated using the formula:

$$r_t = r_d * (a + bcosW)$$

Where a and b are given by

$$a = 0.409 + 0.5016\sin(W_s - 60) \text{ and}$$

$$b = 0.6609 - 0.4767\sin(W_s - 60)$$

The radiation on the collector is increased due to the tilt effect. The effect of the tilt is calculated based on the ratio of total radiation on the tilted plane to the total radiation on a horizontal surface. This translates to the ratio of Cosθ to $Cos\theta_z$ using the following equations as defined by Duffie and Beckman (16);

$$R_b = \frac{Cos\theta}{Cos\theta_z} \text{ where}$$

$$Cos\theta = sin\delta sin\Phi cos\beta - sin\delta cos\Phi sin\beta cos\gamma + cos\delta cos\Phi cos\beta cosW + cos\delta sin\Phi sin\beta cos\gamma cosW + cos\delta sin\beta sin\gamma sinW$$

and

$$Cos\theta_z = cos\Phi cos\delta cosW + sin\Phi sin\delta$$

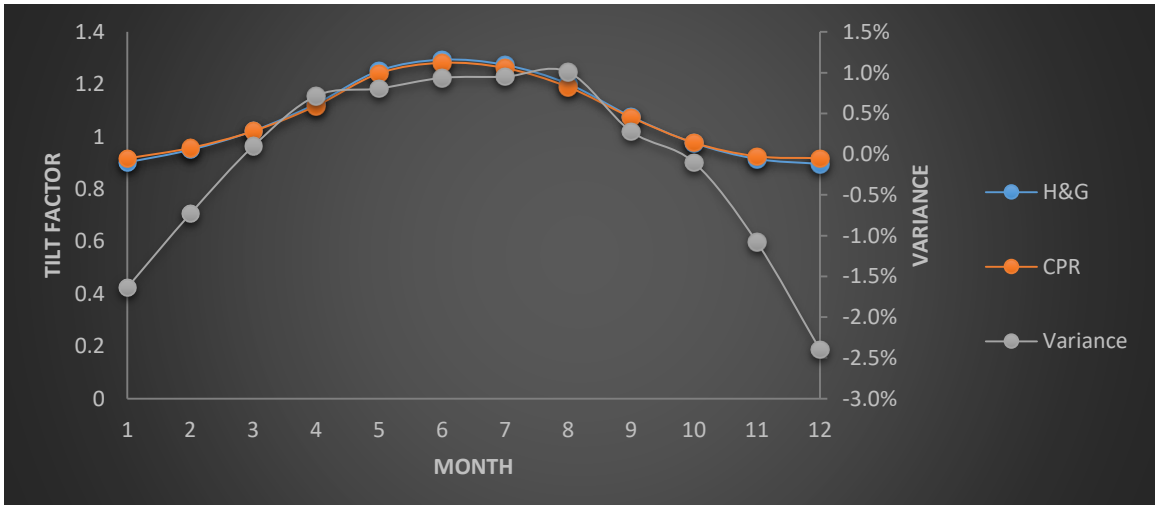

Figure 7:Tilt factor variations at Gweru

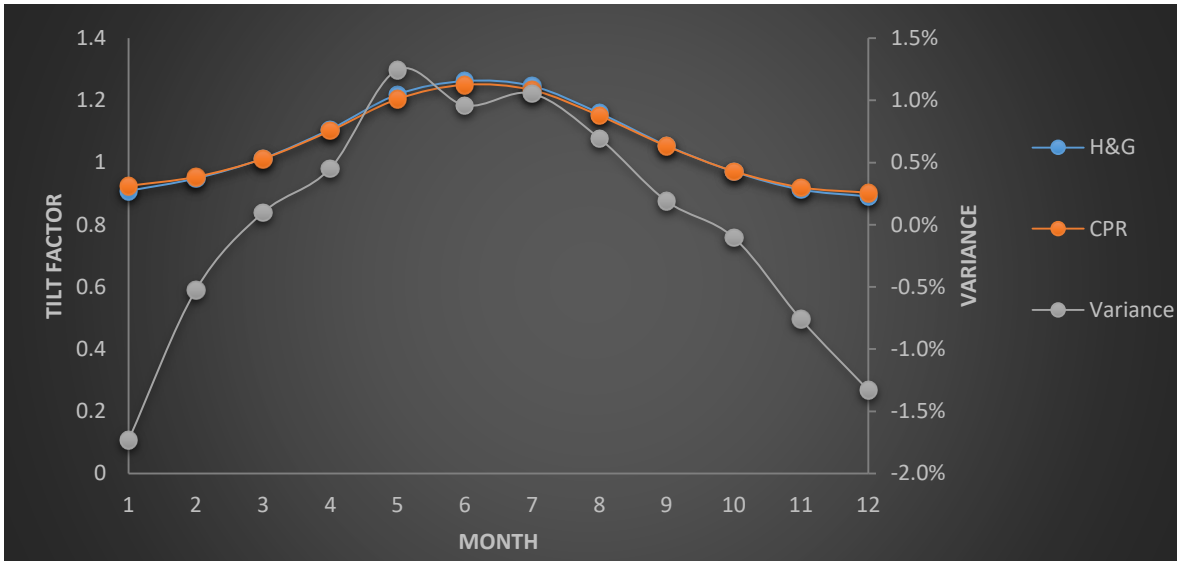

Figure 8:Tilt factor variations at Kariba

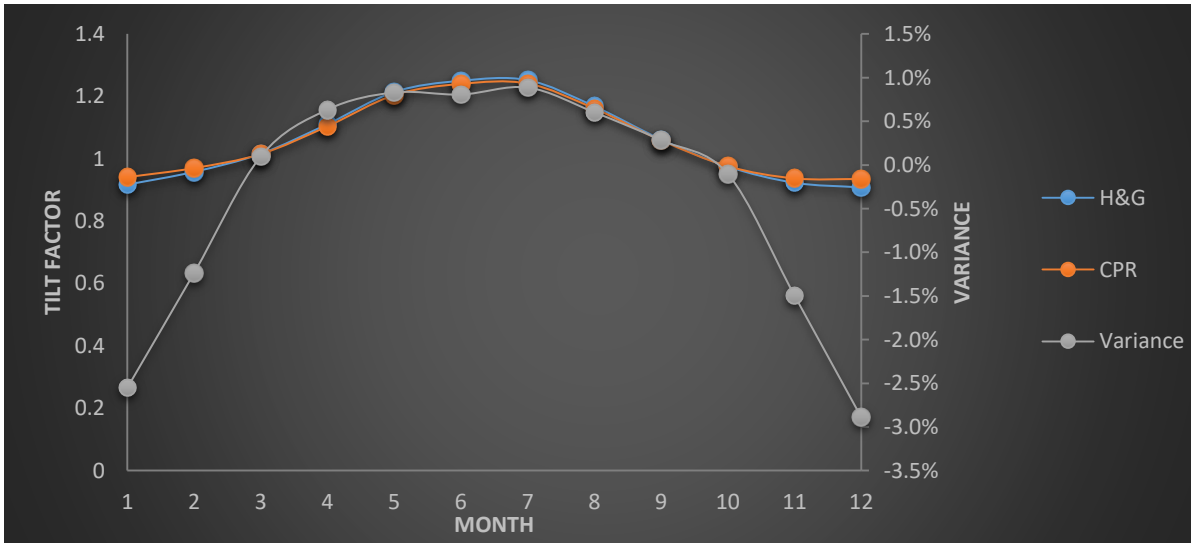

Figure 9:Tilt factor variations at Harare

Finally, the total radiation incident on the collector was calculated based on the simplified Collares-Pereira-Rabl formula as;

$I_T = I_b R_b + I_d$ where I_b and I_d are the beam and diffuse radiation.

The analysis of the collector was based on the following assumptions

i. The heat lost to the ground

ii. Heat gain by the air is homogenous i.e. all the air inside the collector radius is uniform.

iii. Air movement into the collector is uniform.

Two methods were used to determine the convective heat transfer coefficient without using the table that correlates the Nusselt number to the Raleigh Number because of the height between the collector ground and the cover canopy that exceeds the values specified in the graph.

The convective heat transfer function was calculated based on the following procedure:

i. Determination of the Grashof 's number based on the formula

$$Gr = gT_i * \left(T_p - T_a\right) * \frac{r^3}{\mu^2}$$

With $\mu = \left(1.846 - 0.0472 * (T_i - 300)\right) * 10^5$

ii. Determination of the Prandtl number using the formula

$Pr = 1.81 * 10^{-5} * \frac{\vartheta}{C_p}$ for $T_c < 20^o$

$Pr = 1.88 * 10^{-5} * \frac{\vartheta}{C_p}$ for $T_c > 20^o$

The Raleigh number is calculated as a product of the Grashof number and the Prandtl number.

$$Ra = Gr * Pr$$

It is from this Raleigh number that the Nusselt number using the following formula:

$$Nu = 1 + \frac{1.44(1 - (1708\sin 1.8\beta^{1.6}))}{R_a * cos\beta} * \left[1 - \frac{1708}{R_a * cos\beta}\right]^{+} + [\left[\frac{R_a * cos\beta}{5830}\right]^{\frac{1}{3}} - 1\ ]^{+}$$

The convective heat transfer coefficient h_c between the ground and the collector cover is calculated from the Nusselt number as

$h_{c\,(p-c)} = \frac{Nuk}{L}$ where k is the air thermal conductivity and L is the hydraulic length of the collector calculated as $L = \frac{4rh}{r+h}$ were r is the radius of the collector and h is the height of the collector from ground.

The radiation heat transfer coefficient between the ground and the collector cover is calculated using the formula $h_{r(p-c)} = \frac{5.67*10^{-8}*\left(T_{ground}+T_{cover}\right)^2*(T_{ground}+T_{cover})}{\frac{1}{\varepsilon_{ground}}+\frac{1}{\varepsilon_{cover}}-1}$

The radiation heat transfer coefficient from the collector cover to the ambient is calculated using the formula $h_{r\,(c-a)} = \frac{5.67*10^{-8}*\varepsilon_{cover}*(T_{cover}+T_{ambient})^2*(T_{cover}+T_{ambient})(T_{cover}-T_{sky})}{T_{cover}-T_{ambient}}$ and the convective radiation coefficient between the cover and the ambient is dependent on the wind velocity over the cover. Using the formula by Kalogirou 2014 (36)

$h_w = 8.6 * \frac{v^{0.6}}{r^{0.4}}$ where v is the air velocity and r is the radius of the collector.

The top loss coefficient was calculated using the Klein's equation as:

$$U_t = \left[\frac{N}{\frac{C}{T_{ground}}\left[\frac{T_{ground}-T_{ambient}}{N+f}\right]^e} + \frac{1}{h_w}\right]^{-1} + \frac{\sigma(T_{ground}^2 + T_{ambient}^2)(T_{ground} + T_{ambient})}{(\varepsilon_{ground} + 0.00591Nh_w)^{-1} + \left[\frac{2N+f-1+0.133\varepsilon_{ground}}{\varepsilon_{cover}}\right] - N}$$

The back-loss coefficient results in the heating of the ground

The air velocity in the chimney is calculated as $V = \sqrt{2gH_{ch} * (\frac{T_o - T_i}{T_a})}$ m/s. *(Equation 1)*

The air velocity was verified using a mathematical derivation from the useful energy gain:

$$Q_u = A_{coll}F_R(\tau\alpha I_T - U_L(T_{ground} - T_{ambient})) = \dot{m}C_p(T_o - T_i)$$

$$\dot{m} = mass\ flowrate = \rho\dot{V} = \frac{A_{coll}F_R(\tau\alpha I_T - U_L(T_{ground} - T_{ambient}))}{C_p(T_o - T_i)}$$

$$\dot{V} = Volume\ flowrate = vA_{ch} = \frac{A_{coll}F_R(\tau\alpha I_T - U_L(T_{ground} - T_{ambient}))}{\rho C_p(T_o - T_i)}$$

$$V = velocity = \frac{A_{coll}F_R(\tau\alpha I_T - U_L(T_{ground} - T_{ambient}))}{\rho A_{ch} C_p(T_o - T_i)} \text{ m/s} \qquad \textit{(Equation 2)}$$

Table 13: Average Velocity variations in Chimney

Hour Ending	Equation 1 (m/s)	Equation 2 (m/s)	Variance (%)
7	5.287	5.278	0.17%
8	8.245	8.232	0.16%
9	10.094	10.078	0.16%
10	11.434	11.415	0.17%
11	12.308	12.288	0.16%
12	12.723	12.702	0.17%
13	12.675	12.655	0.16%
14	12.157	12.138	0.16%
15	11.241	11.223	0.16%
16	9.829	9.813	0.16%
17	7.810	7.797	0.17%
18	4.613	4.606	0.15%

It can be noted that there was close relation between the results.

The design of a 25kW peak system was done with dimension of:

Table 14:20kW peak design parameters at Kariba

	Option 1	Option 2
Tower height (m)	180	110
Tower radius (m)	5	5
Collector radius (m)	100	130
Ground to cover height (m)	1.85	1.85

Alternatively, design parameters that have a restriction on the height of the tower result in an increase in the radius of the collector as shown by option 2 above. It should be noted that, a reduction in the ground to cover spacing will result in an increase in the peak capacity output. The graph below show the increase in output (kW) against a reduction in the ground to cover spacing.

Option 2 is based on the tallest building in Zimbabwe being the Reserve bank of Zimbabwe at 394 feet (131m) and the second tallest building being Joina City 110m high. Most telecommunication base stations in Zimbabwe have a maximum tower height of 70m (S.I 137 of 2016 Postal and telecommunications (Infrastructure sharing) regulations).

Using option 1, the output of the Solar chimney plant was found to be as shown below:

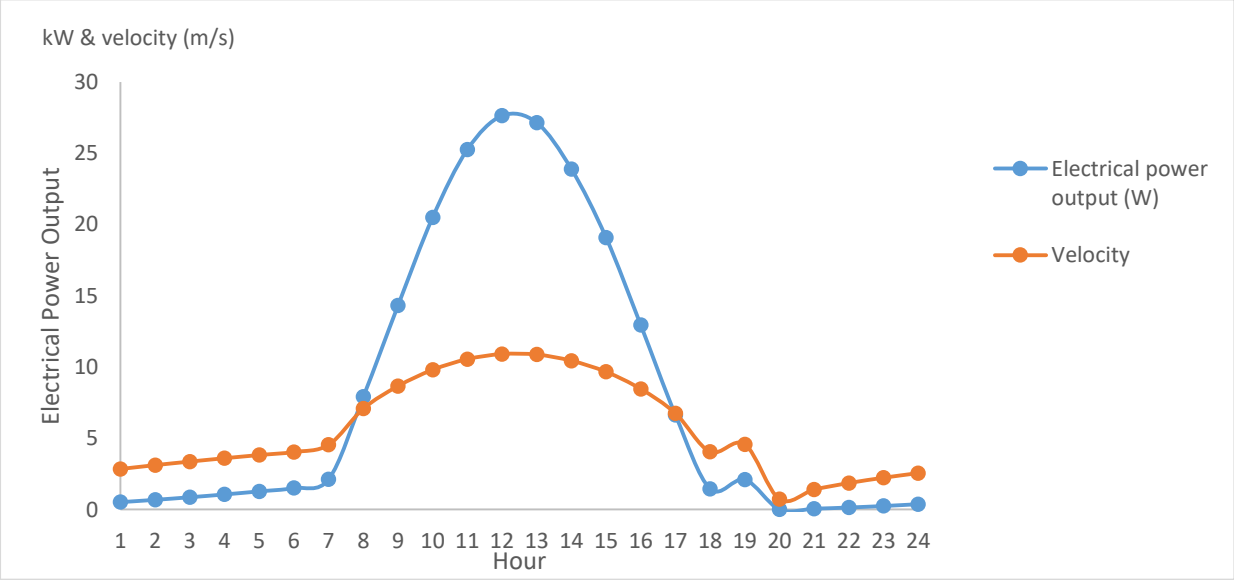

Figure 10:Electrical power output at Kariba in August

From figure 11 above, it can be noted that at 08:00am the plant will be able to generate 7kW and peaks to 27.6kW at 12:00pm. At 17:00 hours the plant will be generating 6.75kW. the plant can generate and meeting the 20kW load from 10:00am and 15:00pm.

Figure 12 below show the monthly variations in the output at Kariba

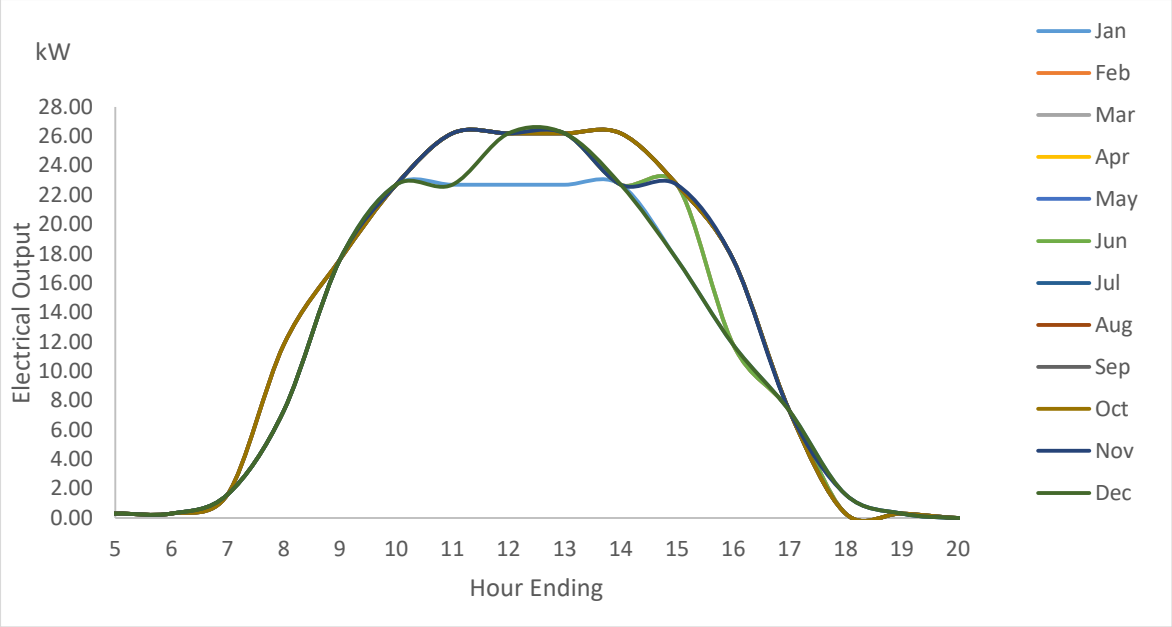

Figure 11:Monthly variations in electrical output at Kariba

When the same plant dimensions are used at Harare and Gweru, the following outputs indicated in Figure 13 and 14 can be achieved.

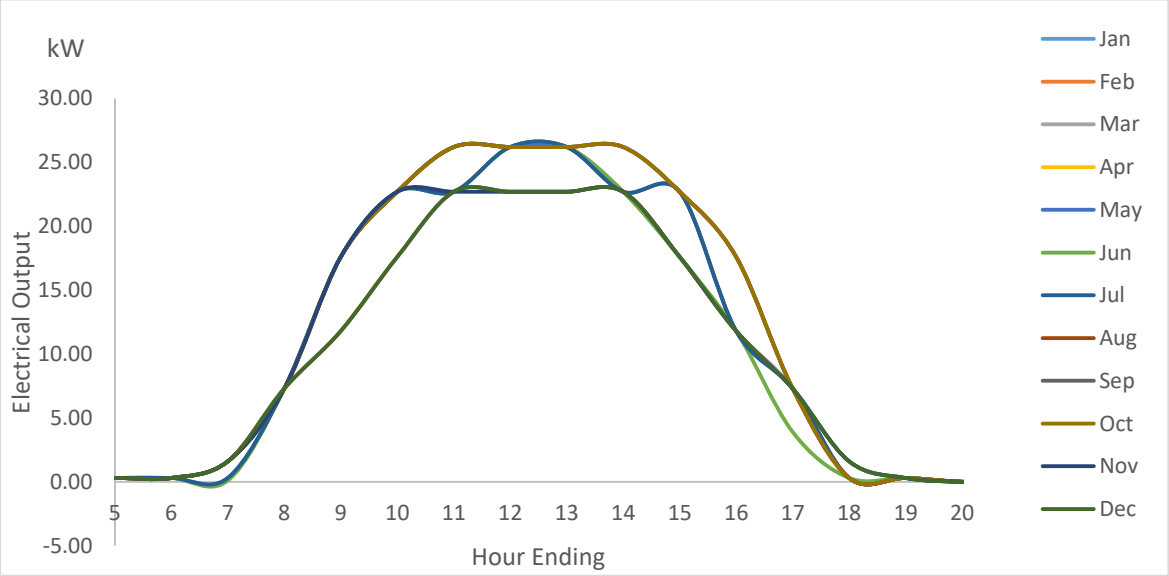

Figure 12:Monthly variations in Electrical output at Harare

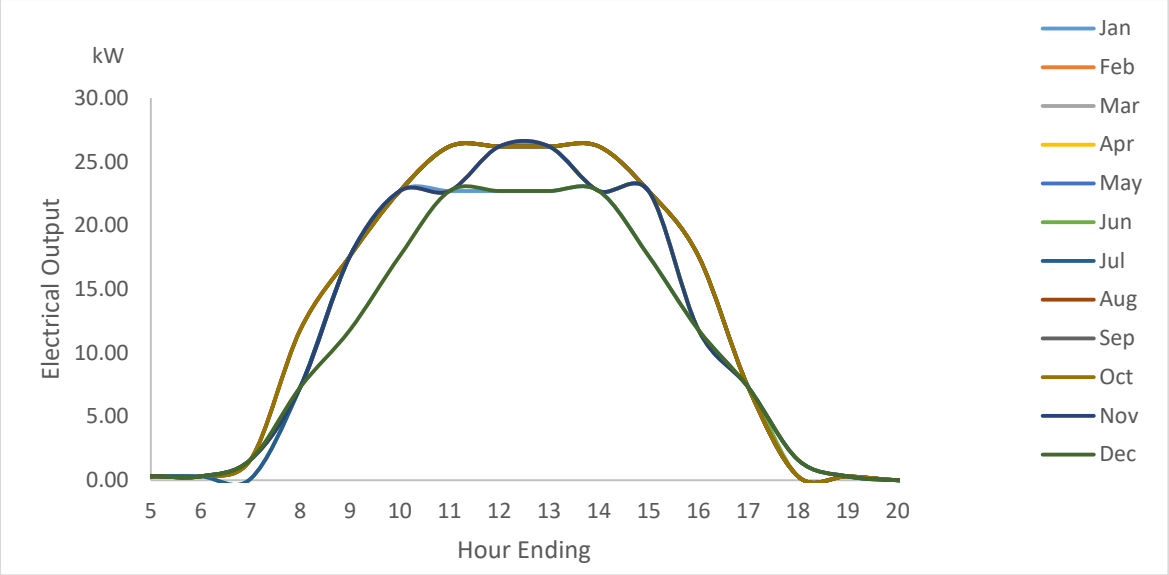

Figure 13:Monthly variations in Electrical power output at Gweru

The peak capacity factor of the plants at the three locations based on the formula $CF = \frac{Energy\ generated}{peak\ capacity * hours\ of\ operation}$ was determined to be 28.9%, 28.2% and 28.9% for Kariba, Harare and Gweru respectively. Figure 15 ,16 and 17 below indicate the monthly variations in the capacity factors for each location.

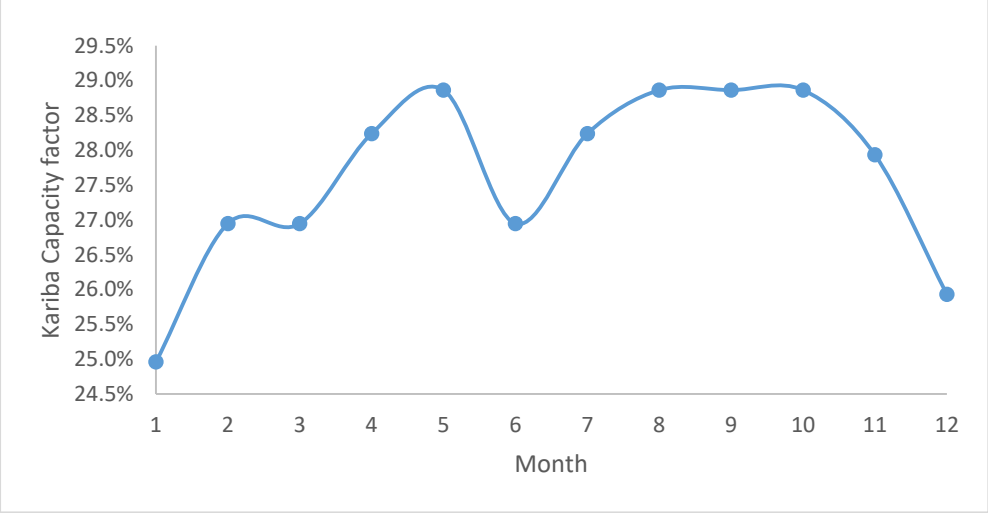

Figure 14:SCPP Monthly capacity factors at Kariba

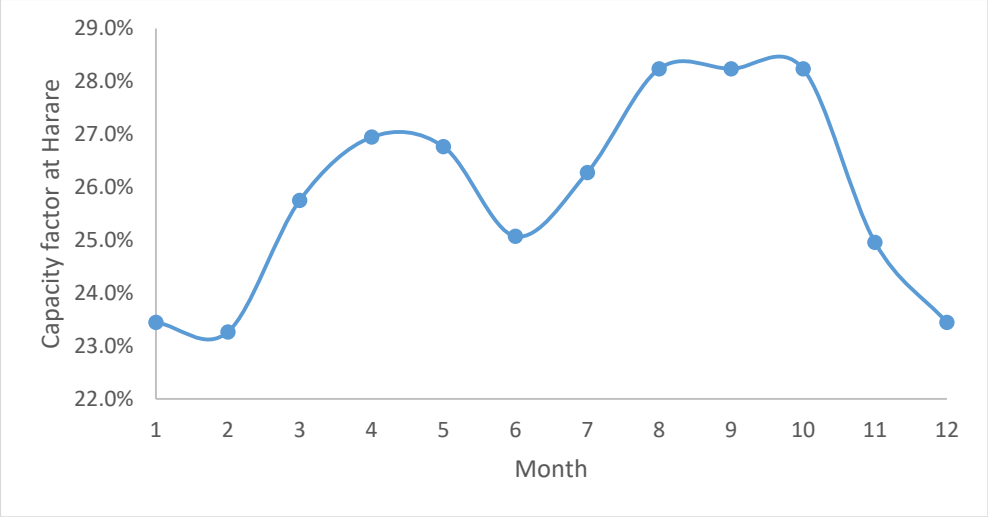

Figure 15:SCPP capacity factor at Harare

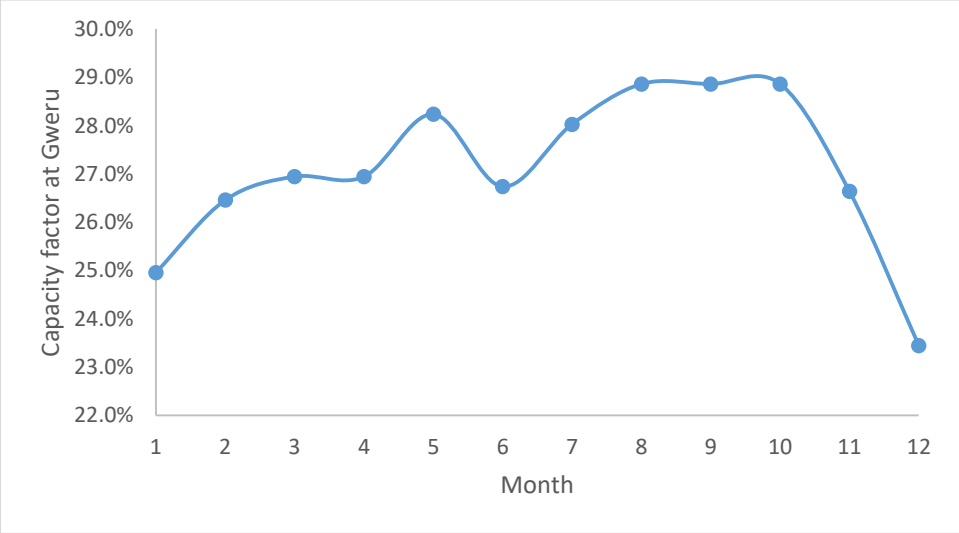

Figure 16:SCPP capacity factor at Gweru

The combined capacity factor trends shown in figure 18 indicate that Kariba has the highest capacity factor.

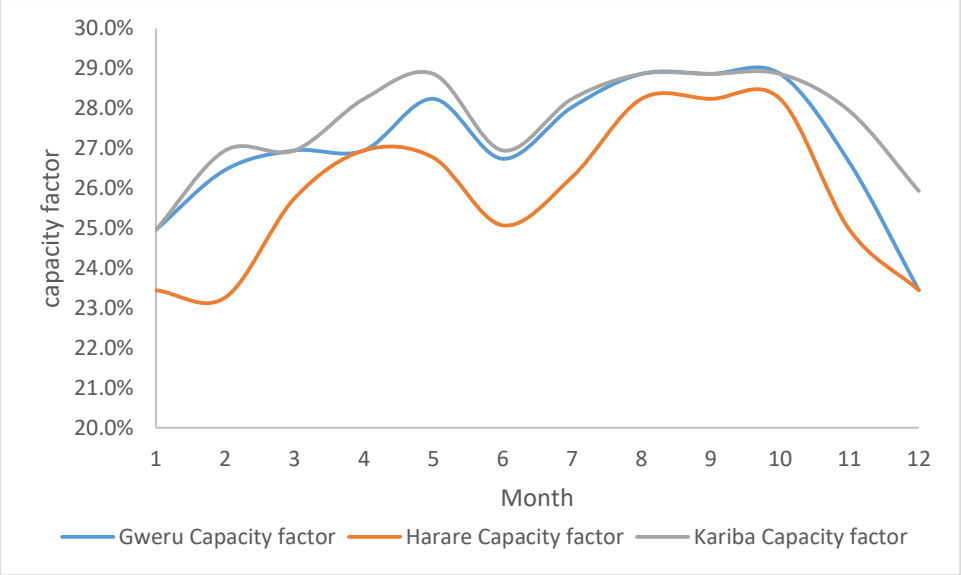

Figure 17:SCPP capacity factor at Kariba, Harare & Gweru

The total energy that can be generated at Kariba, Gweru and Harare was determined as 72,618.1 kWh, 71,176.2kWh and 68071.5kWh. it is evident for these figures that Kariba will generate the maximum energy output followed by Gweru and then Harare.

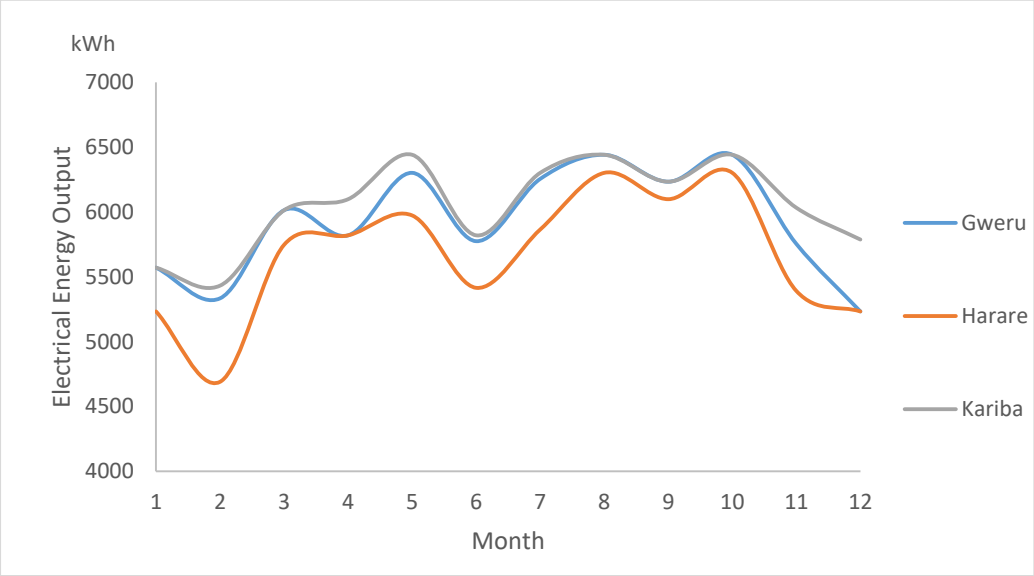

Figure 18:Monthly Electrical Energy Output (kWh)

The collector efficiency was found to be consistent at all three locations. The maximum efficiency of the collector was found to vary with the distance between the ground and the

collector cover. The optimum height was found to be 0.8metres. the efficiency at this height is depicted below:

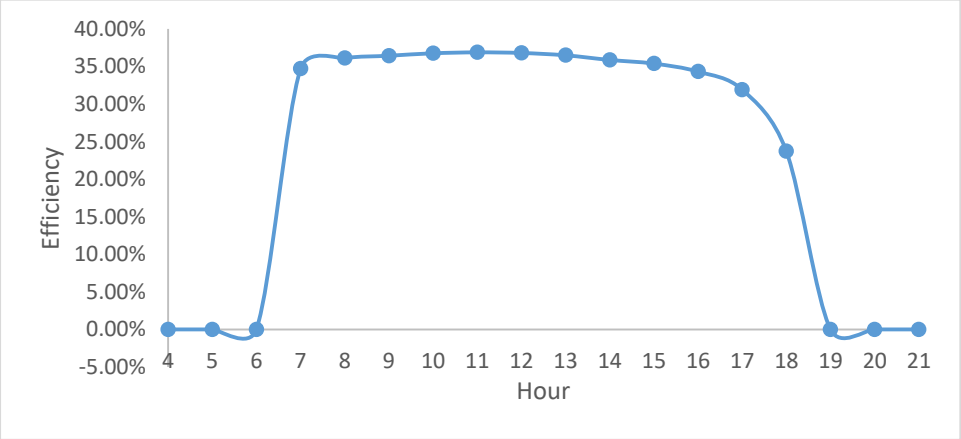

Figure 19:SCPP solar collector efficiency

Chapter 6: Discussion of results

6.1 Tilt factor variations

Plots of the tilt factors from the Hove and Gottsche and the Collares-Pereira- Rabl indicate a high correlation. Variations of less than 3% were noted at both Harare, Kariba and Gweru.

To ascertain the validity of the model, data for the experimental prototype at Manzanares in Spain were input the model and using the Polaris 50kW wind turbine power curve indicated in Figure 21, the results were obtained as indicated in figure 22 and compared to experimental results in figure 23 below:

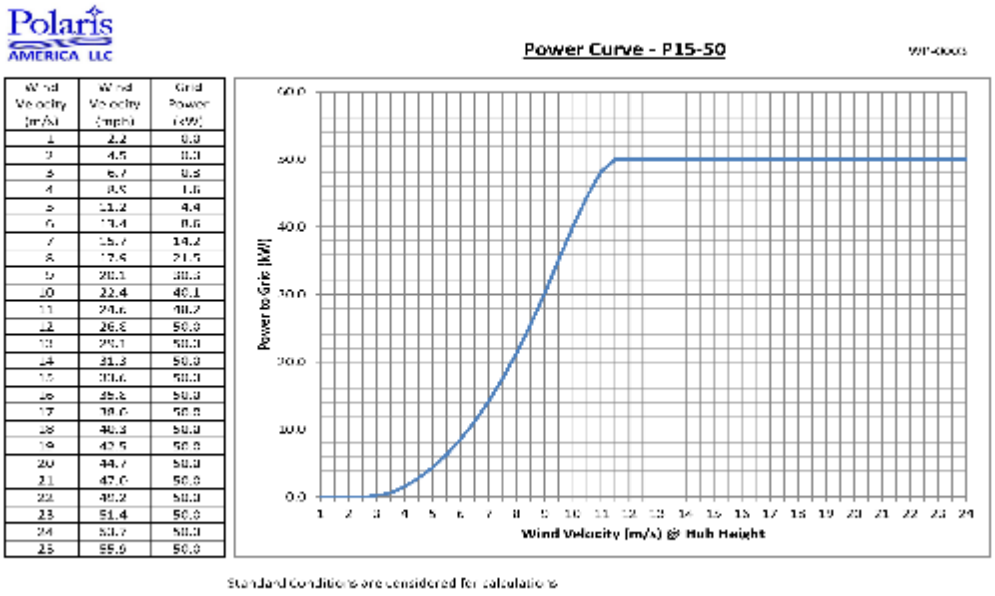

Figure 20:50kW Polaris wind turbine power curve (Polaris America)

The performance equation for the turbine was derived as indicated in table xx below:

Table 15:Performance characteristics of a 50kW Polaris turbine

Air velocity	equation
0-2	0
>2 and <12	$-0.0003x^6 +0.0111x^5-0.1453x^4+1.0006x^3 - 3.1407x^2 +4.2929x -2.0273$
>=12	50

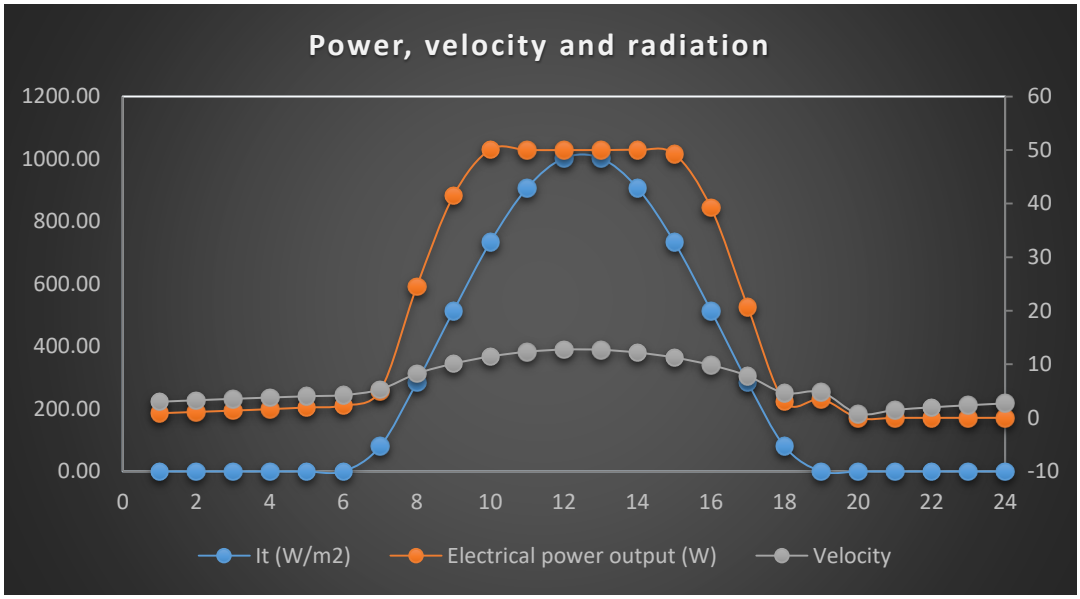

Figure 21:SCPP model output using Manzanares data

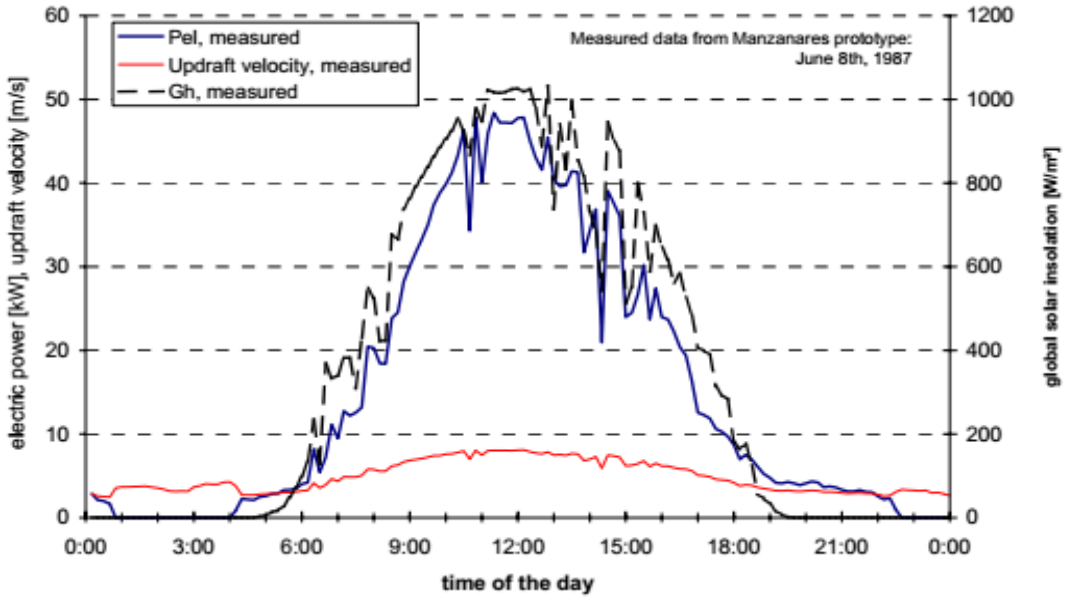

*Figure 22:SCPP plant output test data measured in 1987 *source Schaich et al*

An overview of futuristic power plant as predicted by Schlaich and Bergermann 2011 (33) were also verified with the model. A 50MW plant with dimensions of tower height of 750 m,

tower radius 45 metres and a collector radius of 1875 metres was found to give an output of 45.8MW.

At Kariba it was noted that the maximum output is achieved during the month of May. A peak output of 27.91KW can be achieved during the hour ending 12:00 pm as indicated in figure 24 below. In Harare and Gweru , the peak month is September at 26.08kW and 28.33kW respectively.

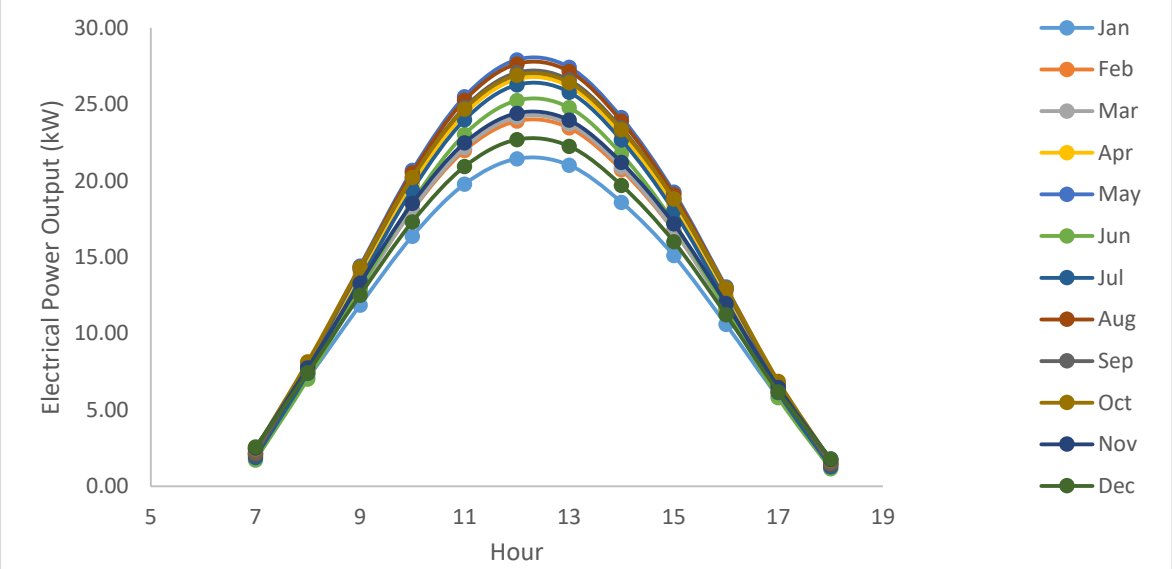

Figure 23:Electrical power output at Kariba

The impact of the chimney was noted to be significant. As noted by other authors the energy output from a SCPP increase significantly with increase in the tower height. Figure 25 below is an analysis of the impact of varying the tower height whilst holding the other components dimensions' constant.

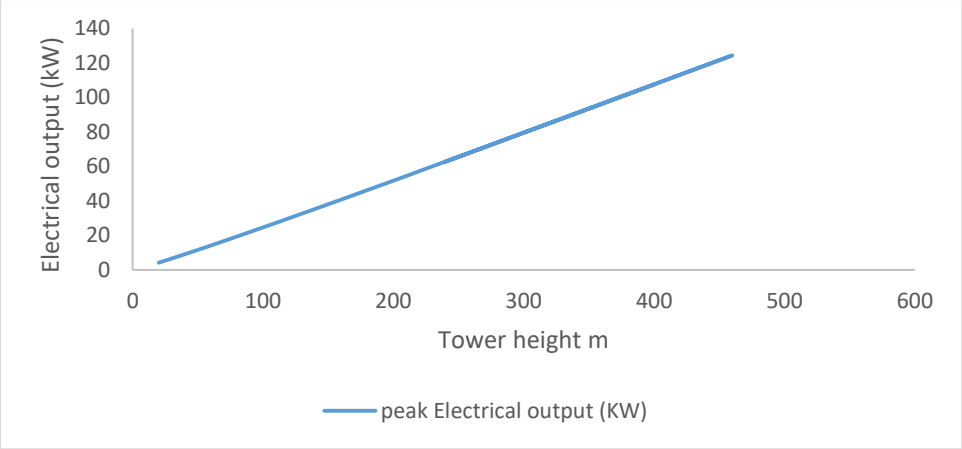

Figure 24:Increase in Electrical output with increase in chimney height

The Zimbabwe weekly and weekend demand profiles is are projected in figure 26 below:

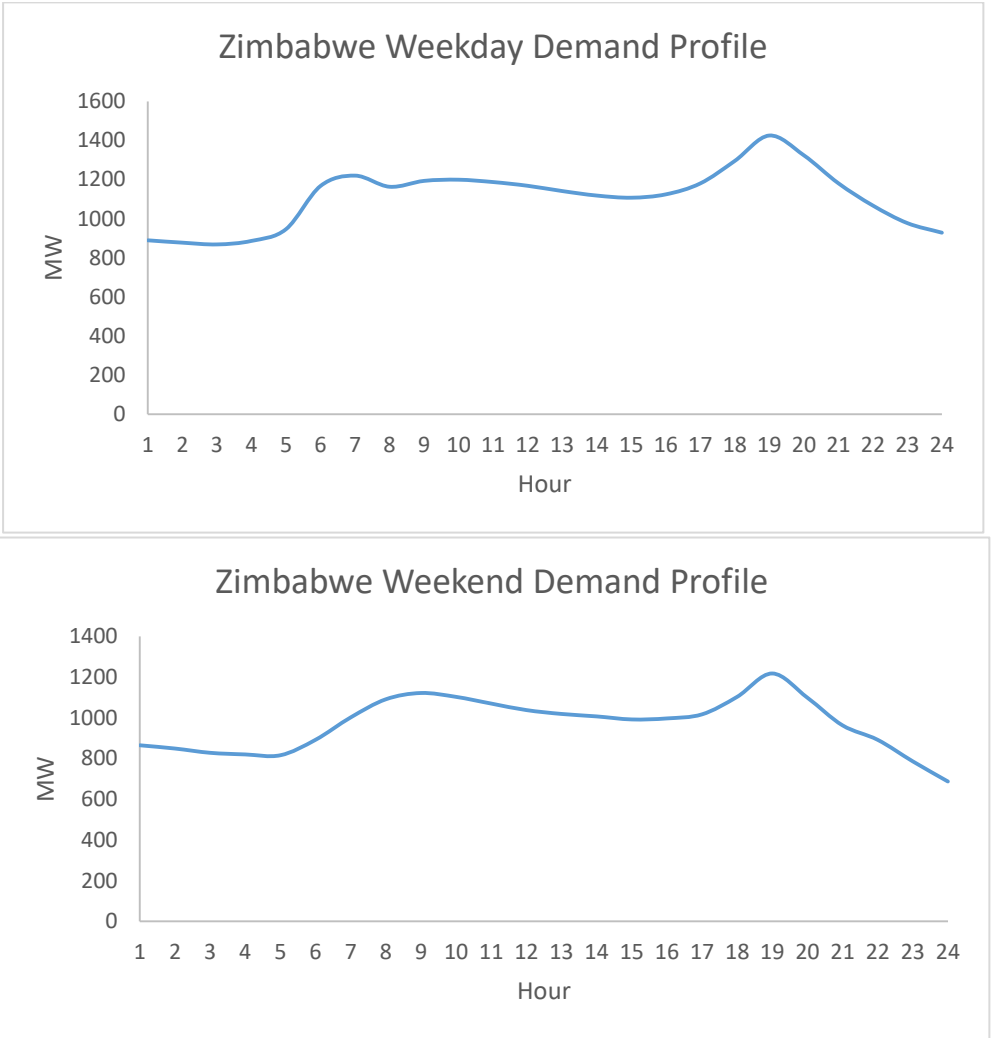

*Figure 25:Zimbabwe Weekday &Weekend demand profiles *Source ZETDC*

The maximum demand for Zimbabwe in 2016 was 1,486MW (ZERA, 2017).Assuming the maximum demand for a community is 25kW, the daily demand profiles can be scaled as shown below:

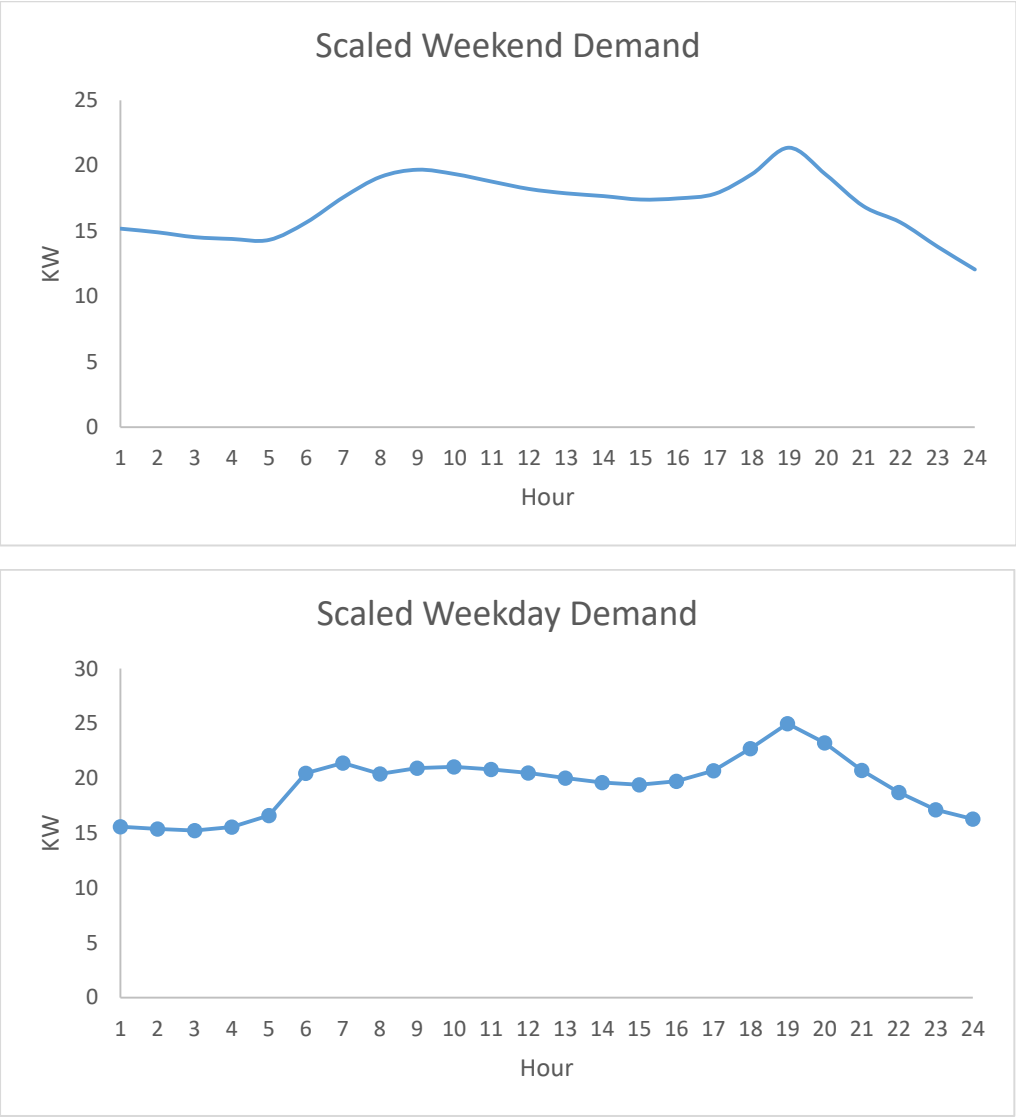

Figure 26:Scaled Weekday & Weekend demand profiles for a 25kWpeak demand community

The SCPP was transposed onto the demand and it can be noted that the above demand can be met from 10:00 am until 3:00 pm. it was also noted that the SCPP can supply 40.6% of the total energy weekday demand and 46.5% during the weekend.

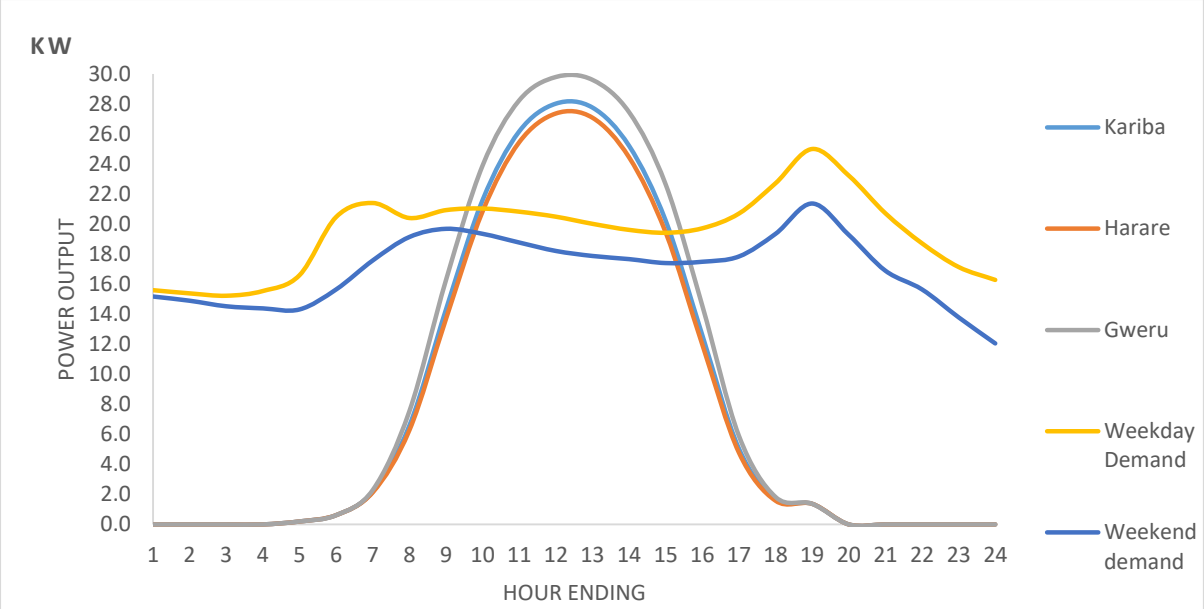

Figure 27:Supply and Demand profiles for an off-grid community

It is evident from the above graph that there is need for storage facilities to enable the SCPP to supply during night time. Thus, a grid tied system or a heat storage facility can be implemented to augment the supply from the SCPP.

6.2 Wind resources assessment in Zimbabwe

To assess whether the SCPP improves the wind resource utilization in Zimbabwe, an analysis was carried out to ascertain the output of the same wind turbine when placed in the open field.

Wind data measurements collected at 10 metre height at Kariba, Harare and Gweru indicate the following hourly average wind speeds as indicated in figures 29 to 31 below. It is evident that Gweru has the highest wind speeds that can peak to 6.7m/s in April whilst Harare and Kariba peak wind speeds are 4.6 m/s in September and 4m/s in October respectively.

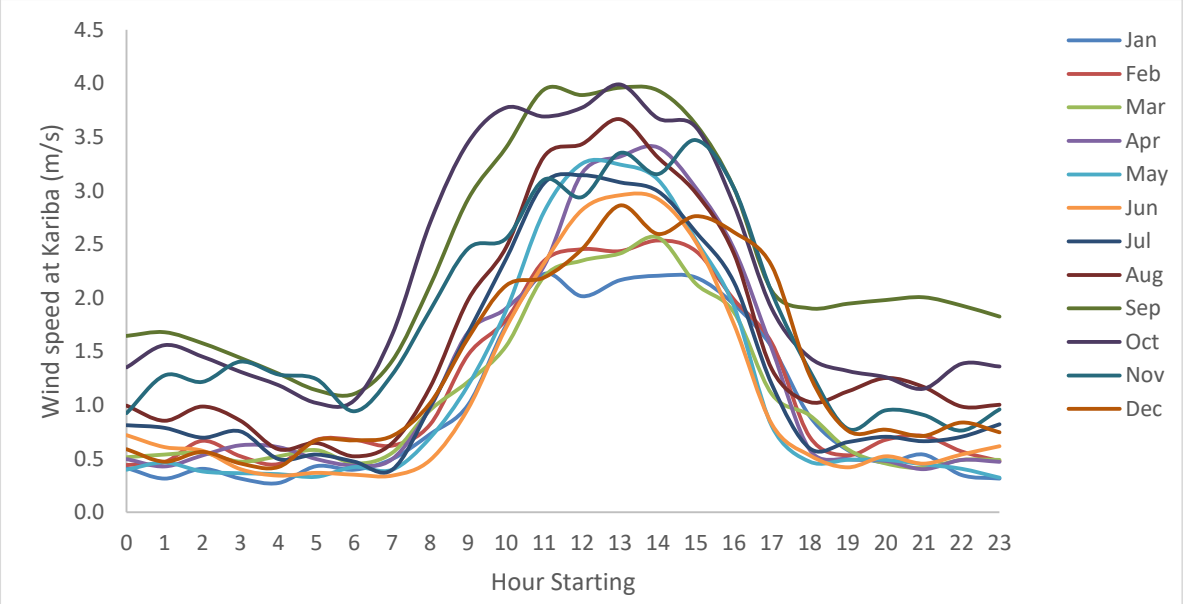

Figure 28: Hourly Wind speed variations at Kariba

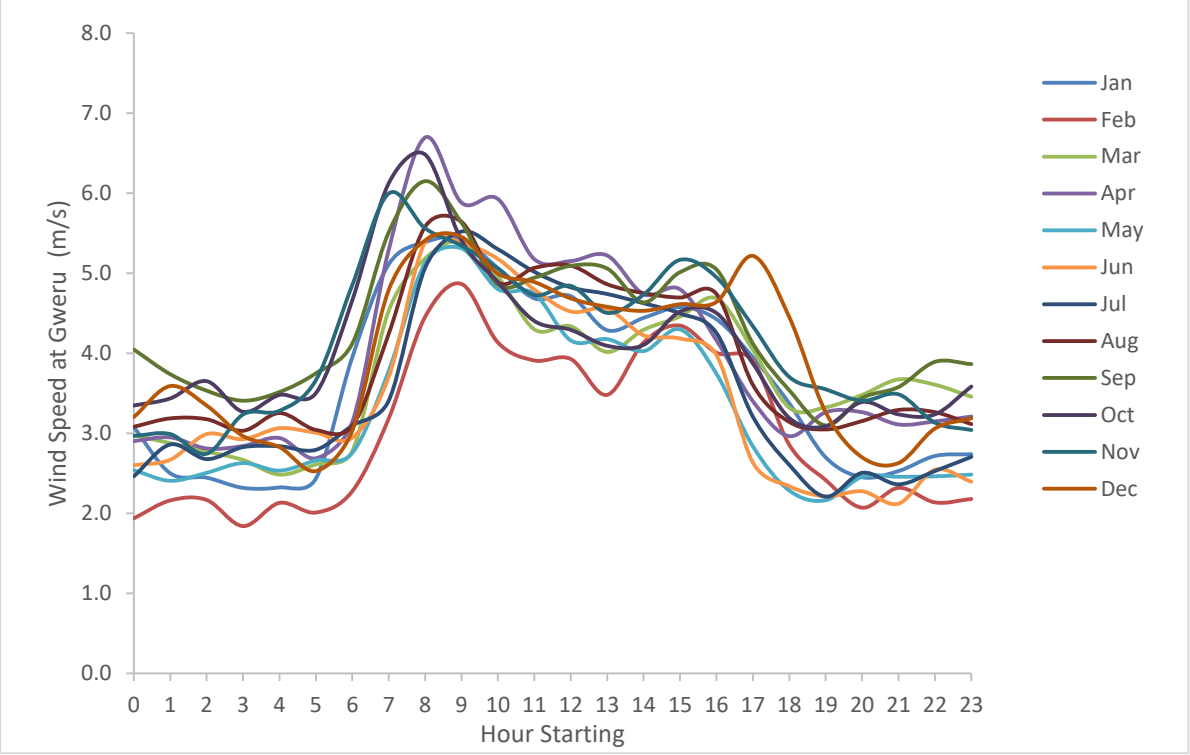

Figure 29:Hourly Wind Speed variations at Gweru

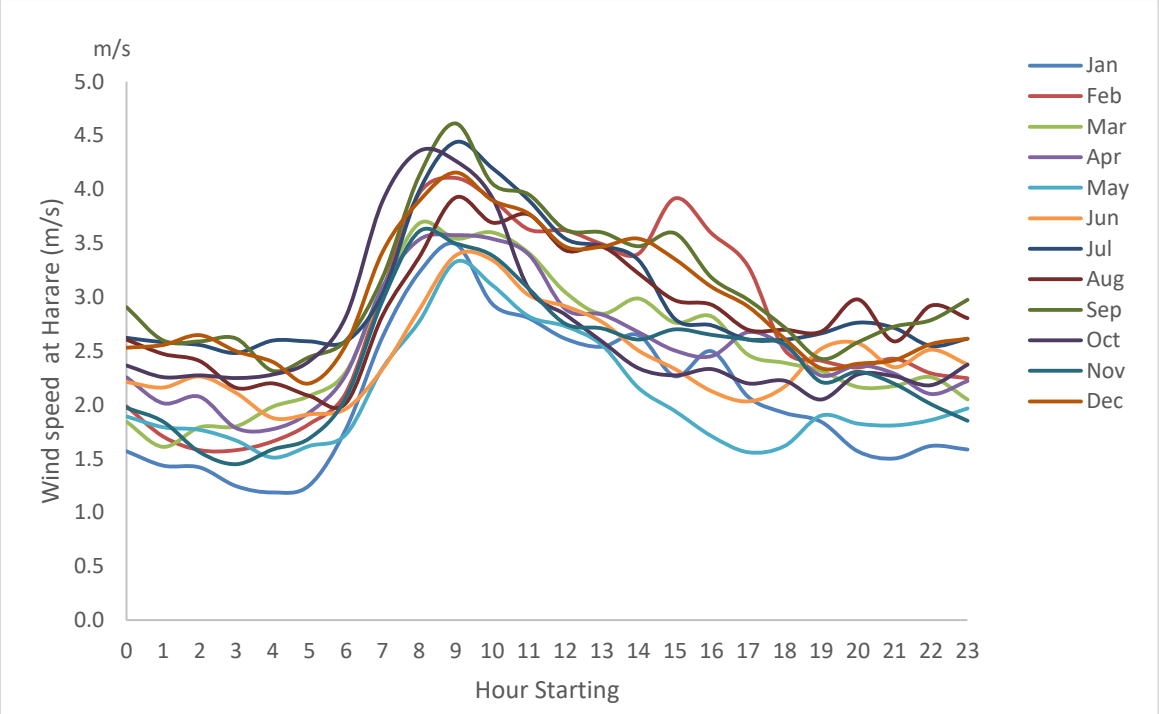

Figure 30:Hourly wind speed variations at Harare

The month of September was found to be consistent among the three places as the peak wind speed month. Using the wind shear equation as defined below and surface roughness of 1.5 for forests and town centres as defined by Sathyajith Matthews 2006 (30), at hub height of 100 metres it is found that the wind speed variations differ as indicated in Figure 30 below.

$$V(Z_{100}) = V(Z_{10}) * \frac{\ln\left(\frac{Z_{100}}{Z_0}\right)}{\ln\left(\frac{Z_{10}}{Z_0}\right)} \qquad where\ Z_0\ is\ the\ roughness\ height$$

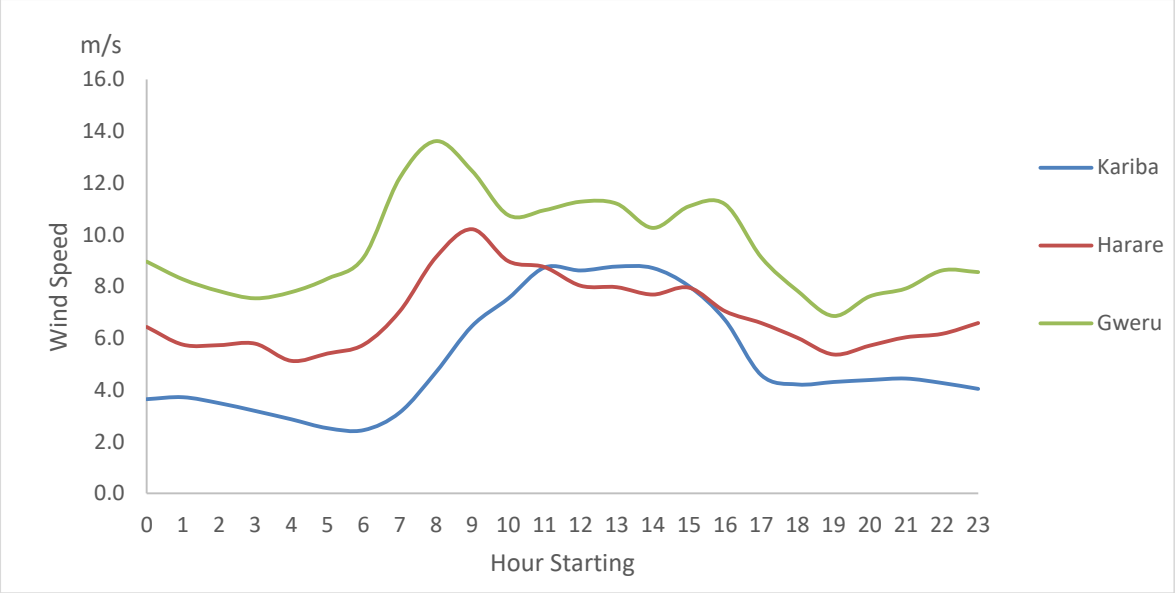

Figure 31: Wind speed variations extrapolated to 100m above ground

The capacity utilisation for a 30kW rated turbine at the three sites was found as shown in Figure 31 below;

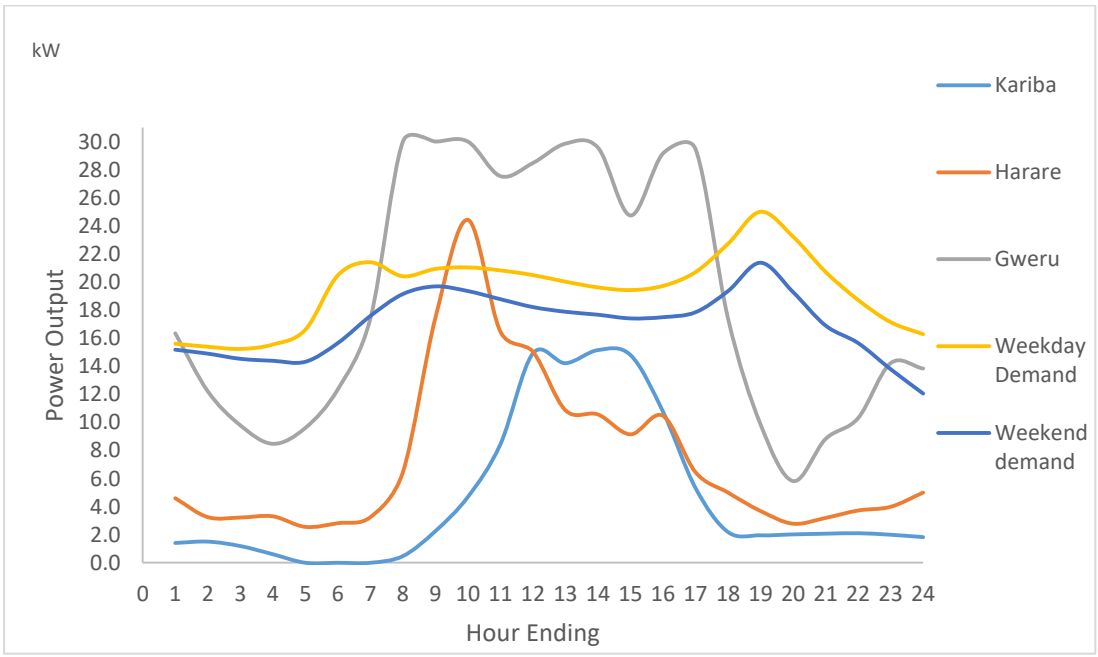

Figure 32:Capacity output of a 30kW turbine at 100m hub height

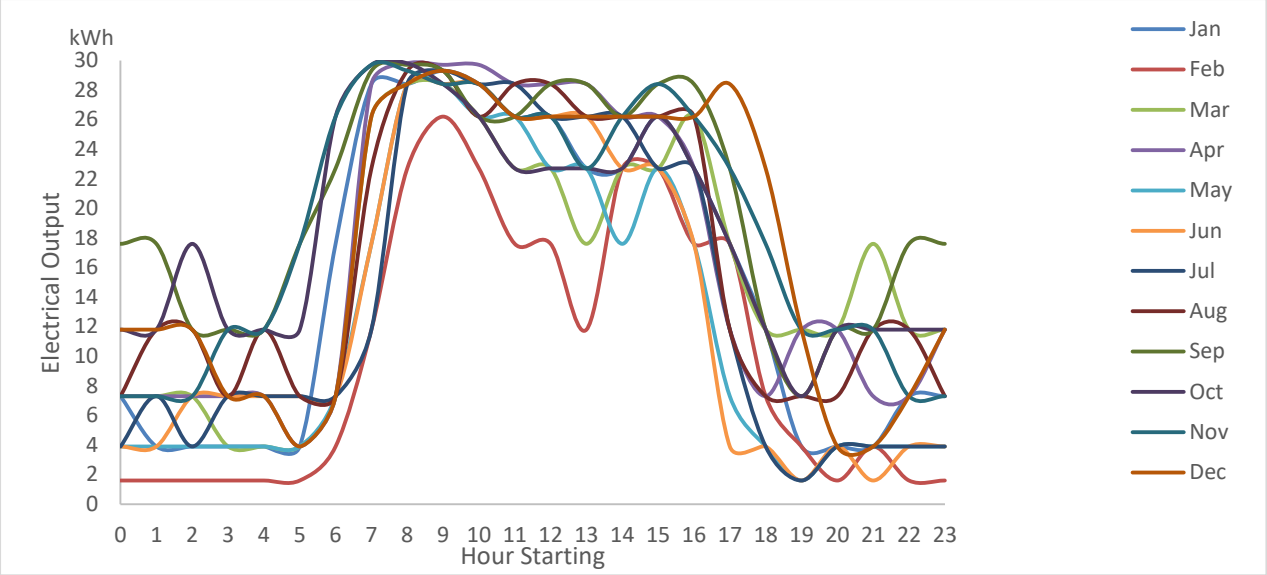

Figure 33:Hourly electrical energy output at Gweru

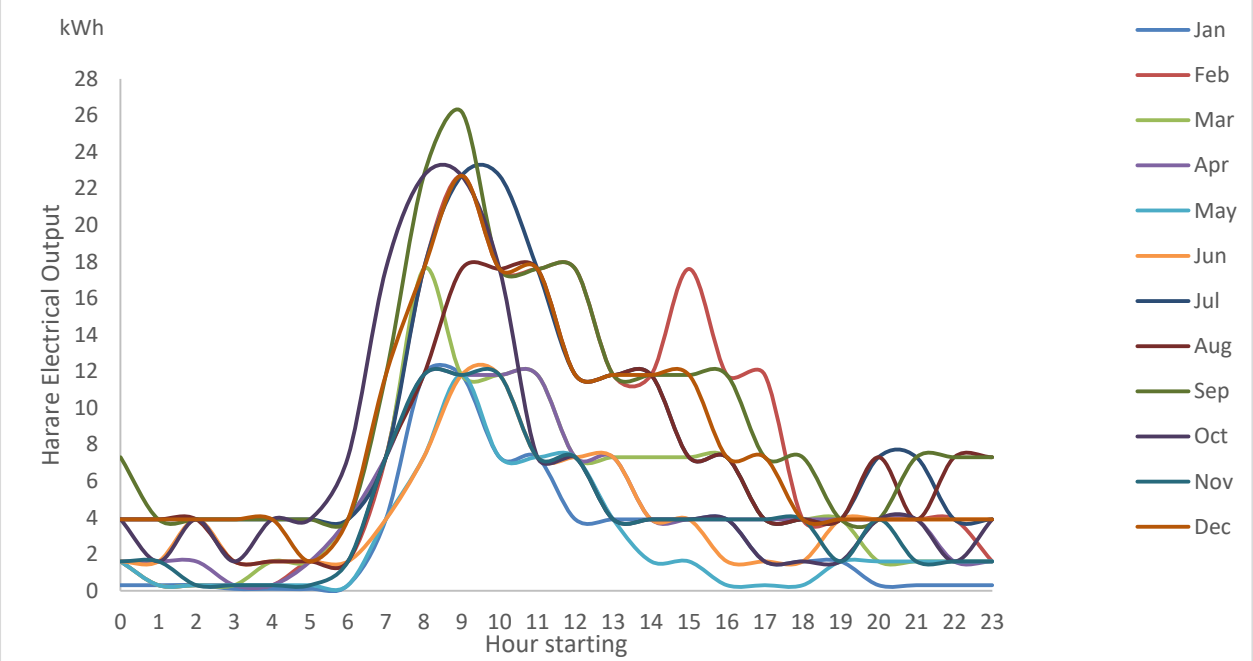

Figure 34:Hourly Electrical Energy Output at Harare

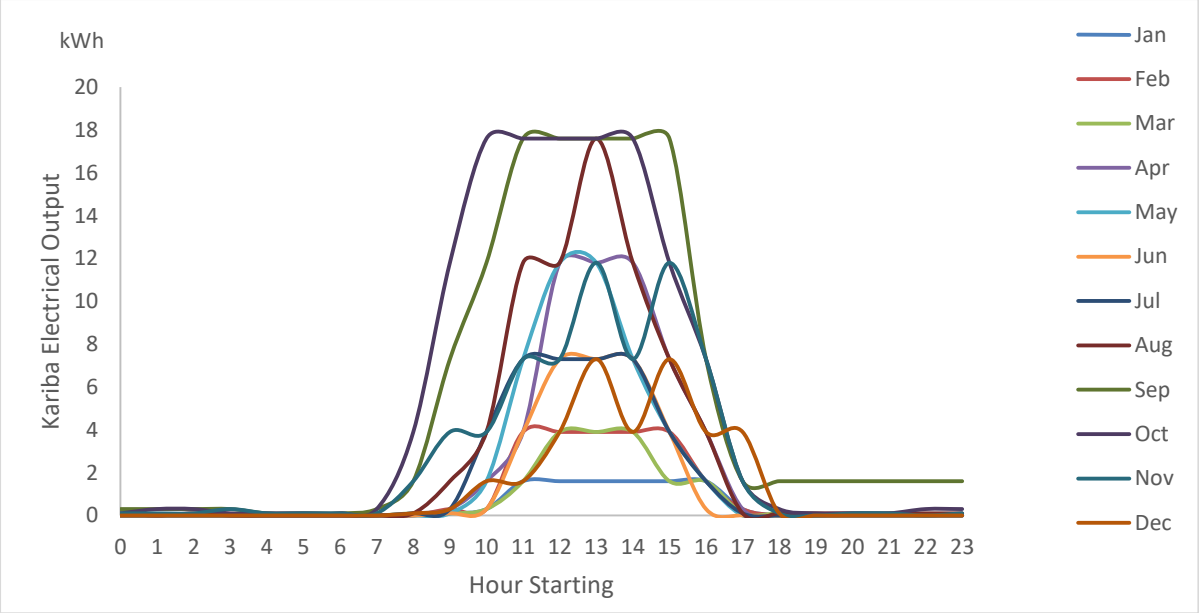

Figure 35:Hourly Electrical Energy Output at Kariba

6.3 40m hub height comparison

The analysis above were done with the assumption of hub heights 100 metres for the open wind turbine. This height is usually associated with turbines of higher magnitude above 10MW. Thus it is not technically and economically feasible and profitable to install a 30kW turbine on a 100 metre hub height.

An analysis of 20kW to 30kW turbines has indicated hub height between 20 metres and 40 metres. The Jonica Impianti 20kW turbine manufactured in Italy whose rotor diameter is 8 metres and has a minimum hub height of 18 metres was used to compare the output of the SCPP that has a chimney height of 40m, chimney diameter of 8.6 metres and collector radius of 130 metres against the turbine in open air at 40 metre hub height.

The power curve equation derived from the turbine data sheet in table 15 below was derived as indicted in table 16:

Table 16: Jonica Impianti 20kW HAWT power curve data

Wind speed (m/s)	Power (kW)	Wind speed (m/s)	Power (kW)

1	0	8	6
2	0	9	8.6
3	0.25	10	11.8
4	0.5	11	15.6
5	1.5	12	20
6	2.5	13	20
7	4	14	20

Table 17:Power equations for the 20kW Jonica Impianti turbine

Velocity (m/s	Power equations
< 3	0
3=< velocity<12	$-0.0004x^4 + 0.0196x^3 - 0.0558x^2 + 0.1752x - 0.3197$
>=12	20

The wind variations and power output from the SCPP for the three locations was determined using the month of September as detailed in figure 36 to figure 38 below.

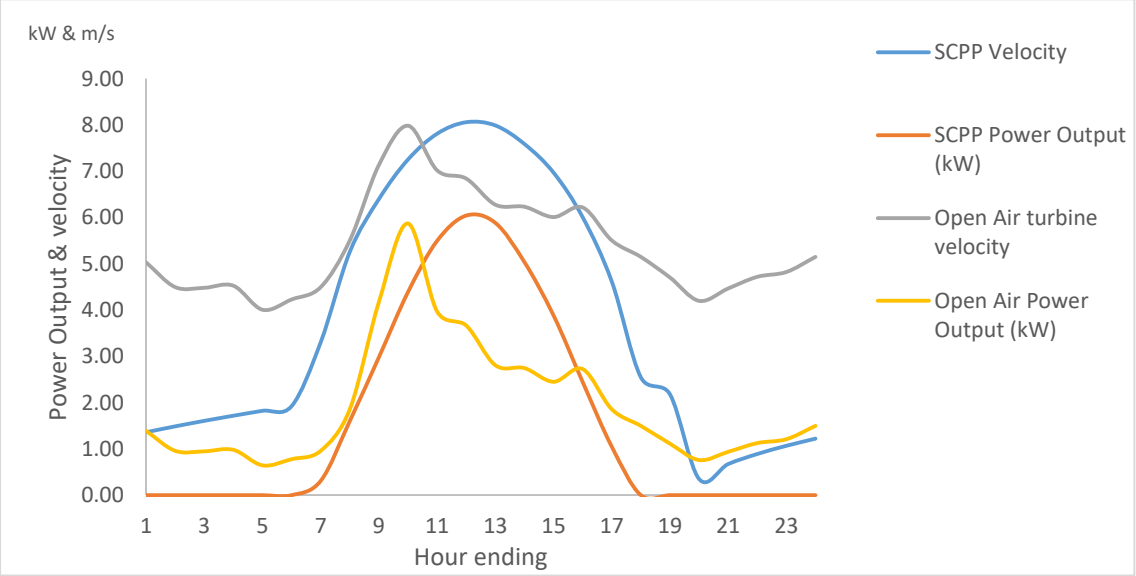

Figure 36:Air velocity and power output at Harare

From figure 36 above, the peak power output of the turbine in open air is slightly lower (5.87kW) compared to the SCPP power output (6.04kW). however, it can be noted that the open air turbine is operating throughout the day whilst the SCPP is limited to operate from 7:00am until 5:00pm.

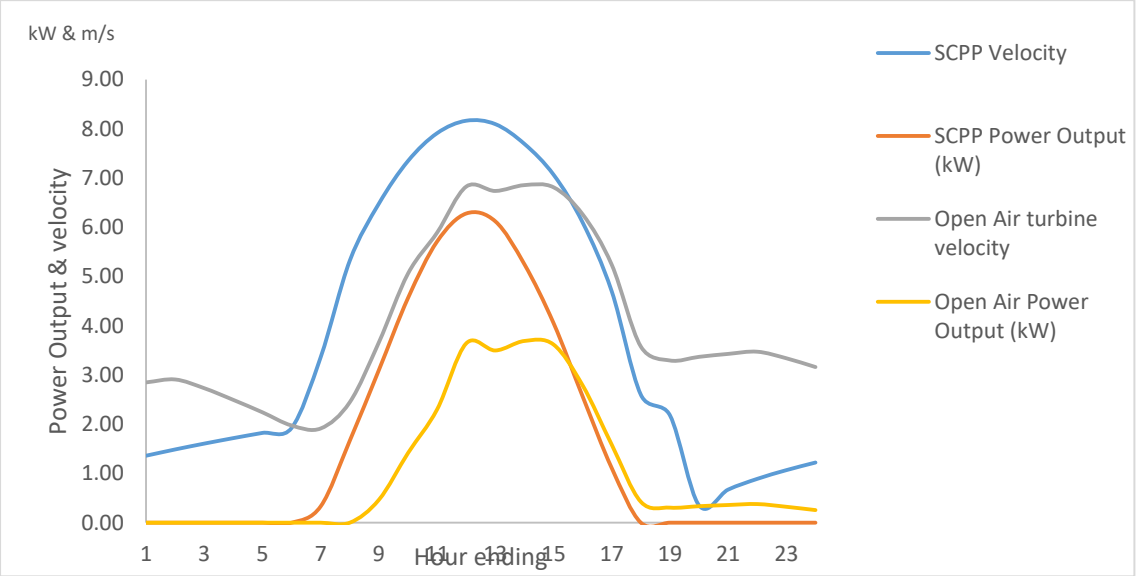

Figure 37:Air velocity & power output at kariba

Figure 37 above indicates that the SCPP plant generates more energy output compared to a 40 metre hub height open-air turbine at Kariba. This has been attributed to the low wind speeds at Kariba.

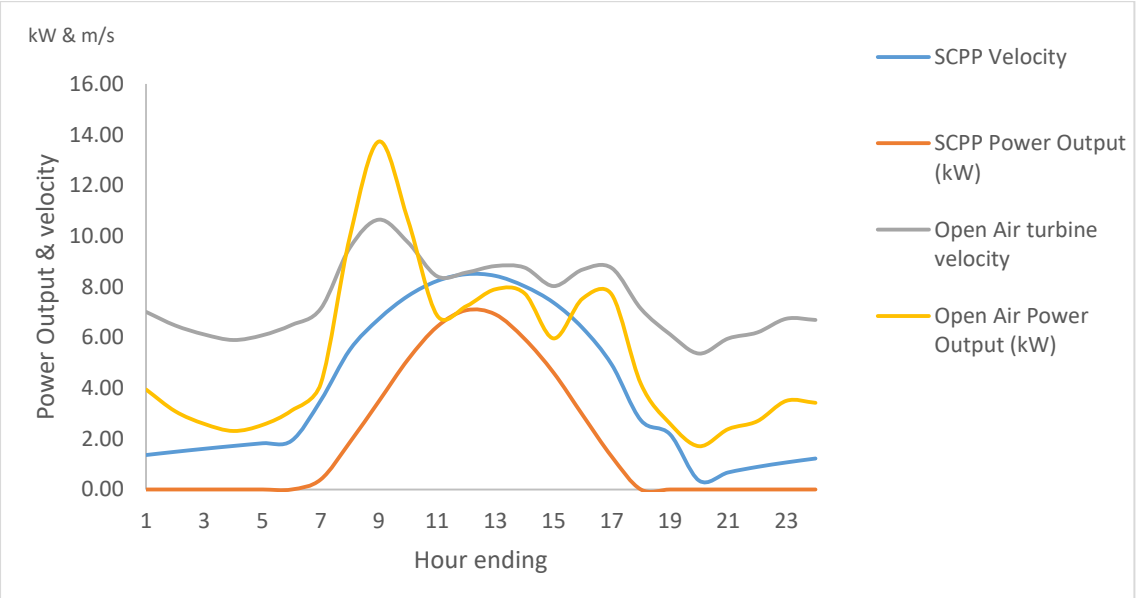

Figure 38:Air velocity & power output at Gweru

At Gweru, the open-air wind turbine produces more energy output when compared to the SCPP. It can also be noted that the peak energy output occurs in the morning.

6.4 Low Radiation Analysis

The analysis above was carried out using the optimistic solar radiation month of September during summer. However, for completeness, the analysis was carried out during the winter period using the month of June.

The incident solar radiation for Harare, Kariba and Gweru are indicated in figure 39 below. Is was noted that despite Gweru being the coldest place during Winter in Zimbabwe, Gweru receives the highest (peak) incident solar radiation of 968W/m^2 when compared to Harare (863 W/m^2) or Kariba (922 W/m^2).

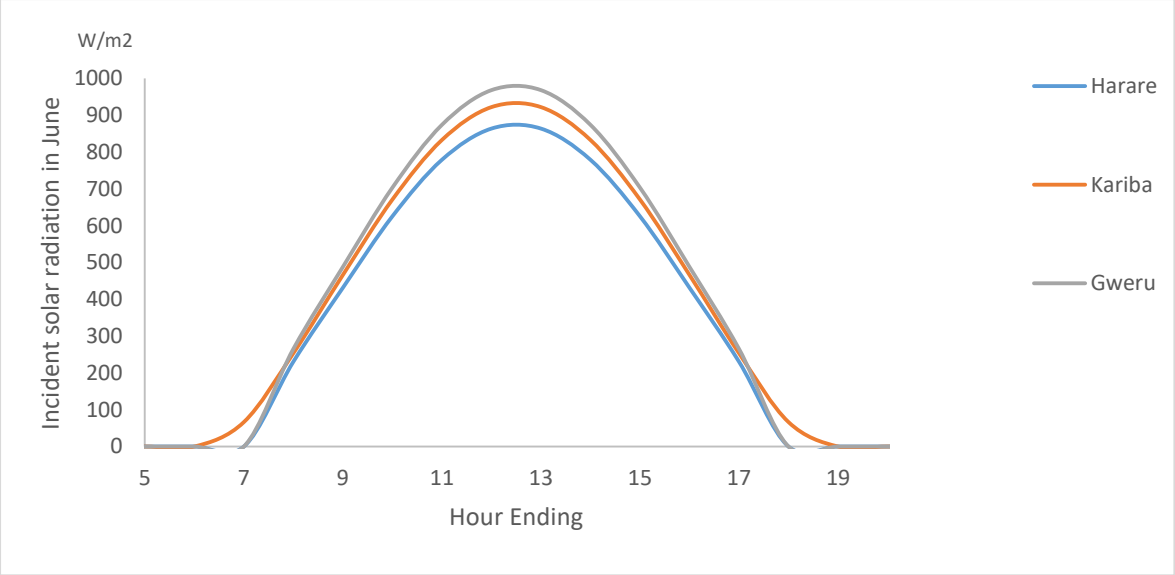

Figure 39:Incident solar radiation during winter period

The daily energy output from an Aeolos 30kW wind turbine are indicated in figure 40 below. It was noted that the SCPP produces more energy output at Gweru with a daily output of 184.96kWhs compared to Kariba which has 178kWhs and Harare 162.62kWhs. This translates to capacity factors of 22.6%, 24.7% and 25.7% at Harare, Kariba and Gweru respectively.

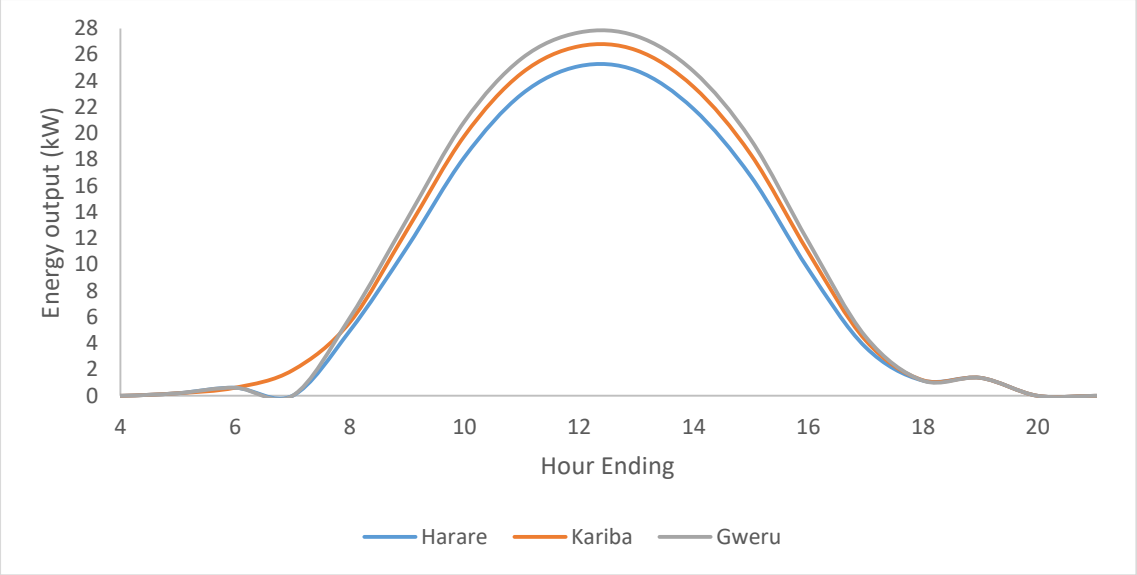

Figure 40: Energy output from an SCPP in Winter

6.4 Analysis Assumptions

The comparison of the SCPP and the Open-air turbine at 100 metres hub height assumed that the air density in both these systems is the same. The air density in the SCPP decreases due to temperature increase whilst for open-air turbines the air density decreases with increase in elevation and temperature. Matthews 2006 (30) indicates the variation of air density with temperature and elevation is given by the equation below.

$\rho_a = \frac{353.049}{T} e^{(-0.034\frac{z}{T})}$ where T is the ambient temperature and Z is the elevation.

The variation between the SCPP air density and the open-air density was found to be less than 1.4% as indicated in figure xx below.

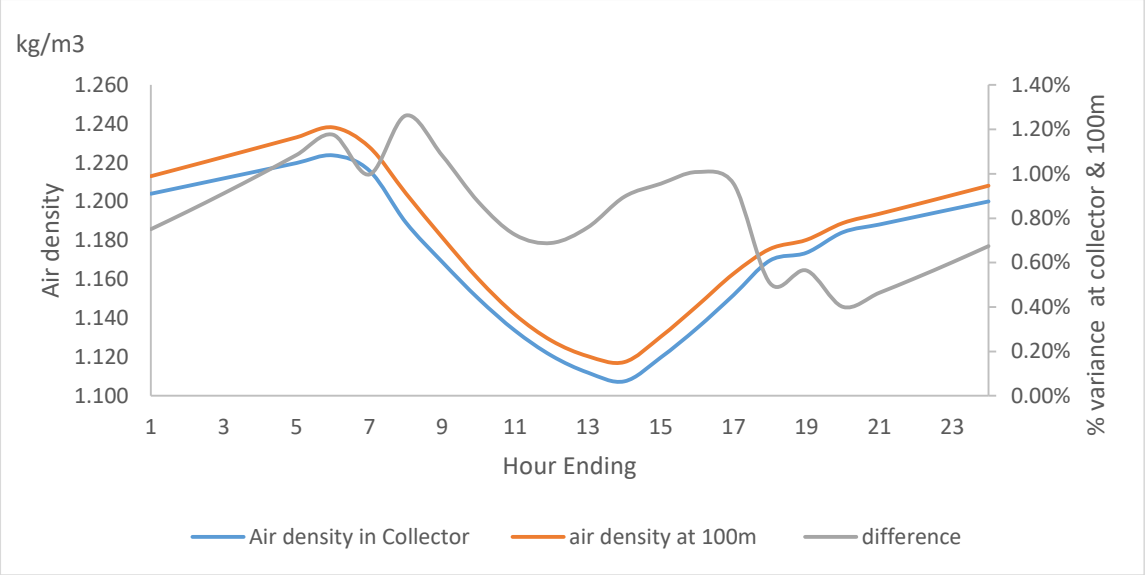

Figure 41:Air density variation between SCPP and Open-air turbine

Chapter 7: Economic Analysis

7.1 Cost components

Solar Chimney Power Plants require capital investments in four main components of tower, collector, turbine-generator and engineering and construction. Schlaich and Bergermann 2011 (33) indicate levelised cost ranges between Euro 0.21/kWh to Euro 0.07/kWh for 5MW and 200MW respectively. It was also indicated that the bigger the SCPP capacity the lower the levelised cost of electricity and the more competitive it is to solar PV.

SCPP have a competitive urge over solar PV or other solar technologies because the materials that are used in the construction are acquired locally making it cheaper.

To supply a 25kW peak demand, a 30kW wind turbine can be installed. Various quotations of 30kW turbine-generator systems range from US$35,000 to US$50,000. IRENA 2012 (38) has indicated that wind turbine prices are steadily decreasing and in 2012 were at $1,400/kW indicated in figure 37 below.

Blanco 2009 gave a capital breakdown of an onshore wind turbine. It was indicated that wind power projects costs consist of four major components that include:

i. Turbine costs composed of hub tower, generator, transformer and turbine blades
ii. Civil works composed of all site preparation and foundation works for the tower
iii. Grid integration costs that enable the wind turbine to be connected to the distribution network; and
iv. Other capital costs which include miscellaneous works including buildings, control systems i.e. SCADA systems and project consultancy costs.

The turbine costs contribute 64% of the total project cost whilst the other components are indicated in figure 40 below. The turbine costs can be further split into components indicated in figure 41 below.

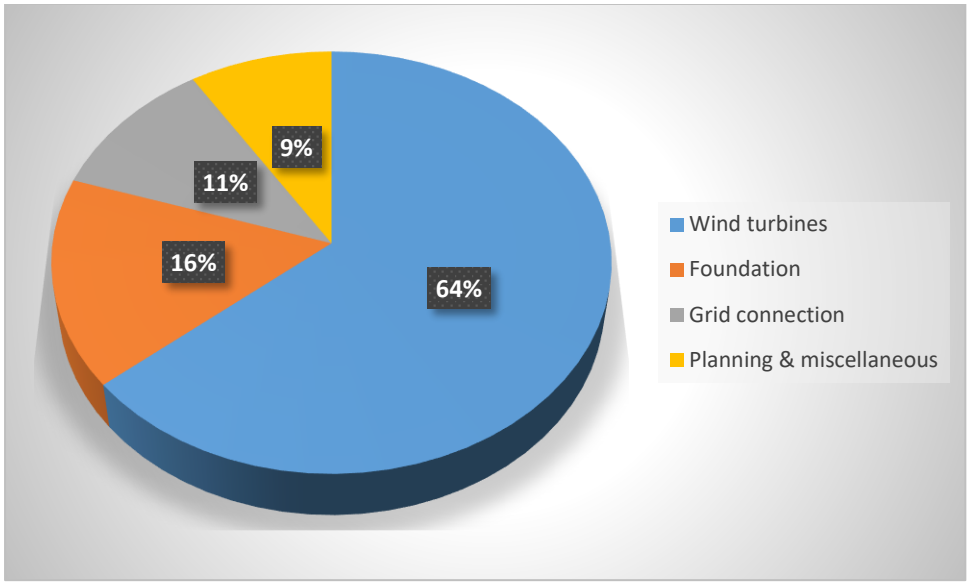

Figure 42: Wind power systems cost components (source Blanco 2009)

Variable costs from 65 projects completed since 2000 has indicated that operation and maintenance cost average $10/MWh (38).

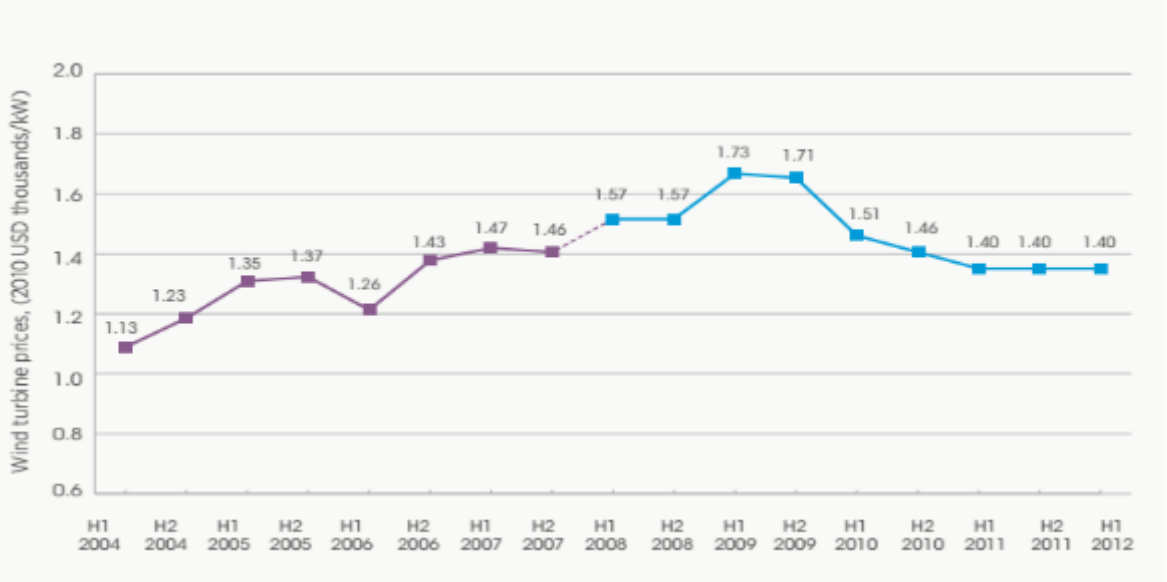

Figure 43:Cost of wind turbine *Source : IRENA 2012

In 1976 the cost of constructing a 108.2m thermal power plant cooling tower was US$2,331,000. Cost components included Materials (concrete, reinforcement, tendons) costing $633,000, labor (precasting, stressing and grouting) at US$300,000, formwork and setup costs at $220,000 and erection costing $500,000 (Zia, 1976).

A report by American tower on the introduction to the tower industry and American Tower gives an insight in the cost of constructing telecommunication towers. In 2010, construction costs in Latin America are approximated to be between $125,000 to $175,000 whilst in India the cost is approximated to range between $40,000 and $60,000 and $225,000 in America for 400 feet lattice towers.

A cost approximation by Lambe et al 2012 (40) indicates a $7.99-$9.41 per square foot. Pack and Mehta 2012 (41) highlighted that a 33.45 m^2 (360 feet) greenhouses was constructed in Tanzania and Kenya for $200.

Table 18:Cost components for a SCPP

Manufacturer	Price
SunSurfs WT3 (30kW)	US$40,000
Tower	US$100,000
Collector ($5/$m^2$)	US$200,000

Total	$340,000
Operational cost per kWh	$0.01

*Labour costs are included in the cost components

The current lending rates in Zimbabwe are capped at 15%. Assuming the plant life is expected to be 20 year. The levelised cost of electricity for the plant when calculated using the formula:

$$LCOE = \frac{\left[\frac{Total\ Investment\ Cost * Discount\ rate}{1-(1+Discount\ rate)^{-Time}}\right]}{Energy\ output} + levelised\ variable\ cost = \frac{\left[\frac{TIC * r}{1-(1+r)^{-T}}\right]}{E} + LVC$$

It was noted that the LCOE will be USc75/kWh, USc73/kWh and USc78/kWh at Gweru, Kariba and Harare respectively. These costs are above grid parity which is currently USc10/kWh for ZETDC and when compared to the ZERA Renewable energy feed in tariffs (Curren, 2016) for plant below 1MW at USc14.0/kWh, it can be concluded that small scale SCPP are expensive for off-grid systems.

If the wind turbine is placed in open air at hub height of 100m, it was noted that the output from the three sites is 137,427.4kWh, 19,589.6kWh and 52,469.6kWh at Gweru, Kariba and Harare respectively. The LCOE assuming the cost components are the turbine, tower construction and Operation and maintenance was calculated as USc17/kWh, USc1.11/kWh and USc42/kWh at Gweru, Kariba and Harare respectively.

It can be noted that the LCOE of SCPP is only cheaper at Kariba and this is attributed to the low electrical energy output of the open wind turbine of 19,589.6kWh when compared to the SCPP plant of 72,618.1 kWh.

Chapter 8: Recommendations and Conclusion

8.1 Recommendations

The study reveal that Solar Chimney Power plants can operate in Zimbabwe especially for off-grid systems in areas where energy resources are scarce considering the abundant solar resource.

The levelised cost of electricity for SCPP is higher compared to grid electricity as well as the REFIT tariff in Zimbabwe hence it is not a possible solution for off-grid electricity supply. However, SCPP should be considered for large capacities of 100kW and above to maximise on land use and chimney heights thus improving the efficiency of the system.

8.2 Conclusion

The study has three main objectives, to assess the solar radiation incident at three selected sites that have varying solar radiation in Zimbabwe which will be used to determine the optimum size of the solar collector diameter, chimney height and diameter to meet a peak demand of 25kW and assess the thermal performance of SCPP when used in at these sites. Parameters such as capacity factor, hourly energy output and efficiency of the system were used as an indicator for suitability.

8.3 Main findings and contributions

i. The radiation mathematical model developed can be used to find the incident solar radiation at ground level for every location in Zimbabwe within a diameter of 50km. The model is capable of to assess the radiation incident at any place in Zimbabwe at both horizontal and tilted planes as well as using various azimuth angles. This data can be used for designing any solar application i.e. Solar PV, solar thermal and SCPP.

ii. SCPP can be developed in Zimbabwe and operated at capacity factors between 20% to 27%. The plants can operate throughout the year.

iii. The energy output from a SCPP was determined at Kariba, Gweru and Harare. However, the output of solar chimney power plants at any location can be estimated using used this model.

iv. SCPP make economic viability in areas were the wind resource is very low. The LCOE at Kariba of USc73/kWh for SCPP is cheaper than an open wind power plant at the same site that comes at a LCOE of USc111/kWh.

8.4 Limitations and suggested future works

i. The mathematical model developed was limited to simulate the performance of the plant during daytime. However, due to the need for energy during the night time there is need to assess the inclusion of heat storage facilities. Salah Larbi et al (Salah Larbi, 2016), Choi et al (Young Jae Choi, 2016), Guo et al (Penghua Guo, 2016) and Papageorgiou (Papageorgiou, 2016) have tried to analyse the performance of SCPP with heat storage with the aim of providing 24 hour electricity supply. Heated water has been cited as a potential candidate for heat storage for such power plants. However, Guo et al have cited different soil types as potential storage mediums.

ii. The accuracy of the model can be improved from the 50km diameter provided radiation data can be extrapolated between the 50km grids used in the model. This will enable a much closer approximation of the SCPP at any location in the country.

iii. The model was verified analytically using data recorded at prototype stations in Spain and found to be correct. However, there is need to use the model to dimension and design a prototype and use various measuring gadgets to verify physical readings against predictions of the model using Zimbabwe radiation data.

iv. Inclusion of temperature data can improve the analysis. In this study the inlet air temperature is assumed to be the same as the ambient temperature. However, the inlet temperature might not be at the same temperature as the ambient temperature.

References

1. (n.d.). *MOEPD - National Energy policy.* 2012, Harare: emagine media.

10. (n.d.). Hove Tawanda and J Gottsche; Mapping global, diffuse and beam solar radiation over Zimbabwe. *Elsevier*, 1999.

11. (n.d.). Ishan Upadhyay, honey Kumar G Vishwakarma, Dr,A,G, BhaveDesign and development of solar chimney. *International Journal of science and research (IJSR)*, 2014.

12. (n.d.). Hamdan Mohammad O, Analysis of a solar chimney power plant in the Arabian Gulf region. *Elsevier*, 2010, 1-6.

13. (n.d.). Rheault, E. Bilgen , Solar chimney power plants for high latitudes. *Elsevier*, 2005.

14. (n.d.). Shashank Thakre, L. Bhuyar, Sachin Dahake and Pankaj Wankhade, Mathematical correlations developed for solar chimney power plant- a critical review. *global journal of researches in engineering*, 2013.

15. (n.d.). P.J Bansod, S.B Thakre and N.A Wankhade, Solar chimney power plant - a review. *International Journal of of modern Engineering research (IJMER)*, 2014, vol 4.

16. (n.d.). *Beckman, John Duffie and William, Solar Engineering of thermal processes.* 2013, New jersey: John Wiley & Sons.

17. (n.d.). Xinping Zhou, Jiakuan Yang, Jinbo Wang, Bo Xiao, Novel concept for producing energy integrating a solar collector with a man made mountain. *Elsevier*, 2009, 847-854.

18. (n.d.). Kumar, M. Augustus Leon and S., Mathematical modelling and thermal performance analysis of unglazed transpired solar collectors. *Elsevier*, 2007,62-75.

19. (n.d.). Ong, K.S., A mathematical model of a solar chimney. *Elsevier*, 2002, 1047-1060.

2. (n.d.). *Oliver Wyman- World Energy trilemma index 2016: Benchmarking the sustainability of national energy systems.* 2016, London: World Energy Council.

20. (n.d.). Jose Manuel Andujar marquez, Miguel Angel Martinez Bohorquez & Sergio Gomez Melgar, Ground thermal diffusivity calculation by direct soil temperature measurement. Application to very low enthalpy geothermal energy system. *MDPI*, 2016.

21. (n.d.). *Florides, Soteris kalogirou and Georgios, Measurements of ground temperature at various depth.* Cyprus: Higher technical institute.

22. (n.d.). *Kusada T Archenbach, Earth temperature and thermal diffusivity at selected stations in the United States.* 1965: ASHRAE.

23. (n.d.). M.A.dos S.Bernardes, A. Vob, G Weinrebe, Thermal and technical analyses of solar chimneys. *Elsevier*, 2003, 511-524.

24. (n.d.). Khandaker Iftekharul Islam, Anisuzzaman Khan and Tanaz Islam, Correlation between Atmospheric temperature and soil temperature: A case study of Dhaka, Bangladesh. *Atmospheric and climate sciences*, 2015, 200-208.

25. (n.d.). Kurpaska, Stawonir, Energy effects during using the glass with different properties in a heated hreenhouse. *Technical sciences*, 2014, 351-360.

26. (n.d.). Ali Hussain, H Al-Kayeim, Aklilu Baheta and Mohammed Aurybi, Comparative critique on the performance evaluation of a solar air heater for mnatural updraft solar system. *ARPN journal of engineering and applied sciences*, 2016, vol 11.

27. (n.d.). Bratucu, Bodolan Ciprian and Gh, Theorectical Research regarding heat transfer between greenhouses and environment. *3rd international conference research and innovation in engineering.* 2014, Brasov, Romania: COMAT.

28. (n.d.). Al-Dabbas, Mohammed Awwad, A proformance analysis of solar chimney thermal power plants. *Thermal Science*, 2011, 619-642.

29. (n.d.). *Pretorius, Johannes Petrus, Solar tower power plant performance characteristics.* 2004, Matieland: University of Stellenbosch.

3. (n.d.). *European Commission, Catalogue of Urban Wind turbine manufacturers.* 2014, European commision.

30. (n.d.). *Sathyajith Mathew, Wind Energy Fundamentals, Reosurce Analysis and Economics.* 2006; Malapuram: Springer.

31. (n.d.). J.C. Roy, S. Wang, C. Kittas & T. Boulard, Convective and ventilation transfers in greenhouses, part 1: the greenhouse considered as a perfectly stirred tank. *Biosystems engineering*, 2002, 1-20.

32. (n.d.). Chitsomboon, Atit Koonsrisuk and Tawit, Mathematical modeling of solar chimney power plants. *Elsevier*, 2012, 314-322.

33. (n.d.). *Bergermann and Schlaich, Solar updraft tower.* 2011, Stuggart.

34. (n.d.). *Commission, European, Catalogue of European Urban Wind Turbine Manufacturers.* Europe: 2016.

35. (n.d.). Menglin Jin, Shunlin Liang, An improved land surface emissivity parameter for land surface models using global remote sensing observations. *American meteorological society*, 2006, 2867-2881.

36. (n.d.). *Kalogirou, Soteris, Solar Energy Engineering processes and systems.* Amsterdam: 2014, Elsevier.

38. (n.d.). *IRENA, Renewable energy technologies: cost analysis series Wind power.* 2012: IRENA.

4. (n.d.). Tawanda Hove , Luxmore Madiye, Downmore Musademba, Mapping wind power density for Zimbabwe: a suitable Weibull-parameter calculation method. *Journal of Energy in Southern Africa*, 2014, Vol 25 No 4.

40. (n.d.). *David P Lambe, Stacy A Adams, Ellen T Paparozzi, Estimating construction cost for low cost Quonset -stylegreenhouse.* Nebraska: 2012, University of Nebraska.

41. (n.d.). Mehta, Min Pack and Khanjan, design of affordable greenhouses for east Africa. *researchgate*, 2012.

5. (n.d.). Takmil Sakir; Baizid Khan Piash ; Shamim Akhter, Design, construction and performance test of a small solar chimney power plant. *Global Journa of research in engineering*, 2014.

6. (n.d.). Omri, Amel Dhahri & Ahmed, A review of solar chimney power generation technology. *International Journal of engineering and advanced technology (IJEAT)*, 2013.

7. (n.d.). Jorg Schlaich, Rudolf Bergermann, Wolfgang Schiel and Gerhard Weinrebe; Design of commercial solar updraft tower system- utilization of solar induced convective flows for power generation. 1997.

8. (n.d.). Fei Cao, Huashan Li, Liang Zhao, Tianyang Bao & Liejin Guo; Design and simulation of the solar chimney power plants with TRNSYS. *Elsevier*, 2013; 23-33.

9. (n.d.). Oboetswe Motsamai, Lesedi Bafetanye, Kobamelo Mashaba & Oaitse Kgaswane; Experimental Investigation of Solar chimney power plant. *Journal of energy and engineering*, 2013, 1980-1984.

Curren, J. (2016). *Updating of Key parameters for data for the Zimbabwean Renewable Energy feed-in tariff.* Harare: ZERA.

Papageorgiou, C. (2016). Enclosed solar chimney power plants with thermal storage. *Science research*, 1-18.

Penghua Guo, Y. W. (2016). thermodynamic analysis of a solar chimney power plant system with soil heat storage. *Elesevier*, 1076-1084.

Salah Larbi, A. B. (2016). Solar chimney power plant with heat storage system performance analysis in South Algeria. *IEEE*.

Tan Yong kwang, A. (2013). *Performance evaluation of solar chimneys in the tropics.* National University of Singapore.

Young Jae Choi, D. H. (2016). Development of analytical model for solar chimney power plant with and without water storage system. *Elsevier*, 200-207.

ZERA. (2017). *ZERA 2016 Annual report.* Harare: ZERA.

Zia, S. R. (1976). *Segmentally constructed prestressed concrete hyperboloid cooling tower.* Manitoba: North carolina State University.

Appendix 1: Thermal properties of various ground soils

Table 19:Thermal properties of various soils

Rock Type	Thermal Conductivity (W/mK)			Volumetric heat Capacity (MJ/m^3K	Thermal Diffusivity (10^6 m^2/s)		
	Min	Typ	Max		Min	Typ	Max
Basalt	1.3	1.7	2.3	2.6	0.5	0.65	0.88
Greenstone	2	2.6	2.9	2.9	0.69	0.9	1
Gabbro	1.7	1.9	2.5	2.6	0.65	0.73	0.96
Granite	2.1	3.4	4.1	3	0.7	1.13	1.37
Peridotite	3.8	4	5.3	2.7	1.41	1.48	1.96
Gneiss	1.9	2.9	4	2.4	0.79	1.21	1.67
Marble	1.3	2.1	3.1	2	0.65	1.05	1.55
Mica dust	1.5	2	3.1	2.2	0.68	0.91	1.41
Shale sedimentary	1.5	2.1	2.1	2.5	0.6	0.84	0.84
Limestone	2.5	2.8	4	2.4	1.04	1.17	1.67
Loam	1.5	2.1	3.5	2.3	0.65	0.91	1.52
Quartzite	3.6	6	6.6	2.2	1.64	2.73	3
Salt	5.3	5.4	6.4	1.2	4.42	4.5	5.33
Sandstone	1.3	2.3	5.1	2.8	0.46	0.82	1.82
Siltstones and argillites	1.1	2.2	3.5	2.4	0.46	0.92	1.46
Dry gravel	0.4	0.4	0.5	1.6	0.25	0.25	0.31
Water Saturated gravel	1.8	1.8	1.8	2.4	0.75	0.75	0.75
Dry sand	0.3	0.4	0.55	1.6	0.19	0.25	0.34
Water saturated sand	1.7	2.4	5	2.9	0.59	0.83	1.72
Dry clay/silt	0.4	0.5	1	1.6	0.25	0.31	0.62
Water saturated clay/silt	0.9	1.7	2.3	3.4	0.26	0.5	0.68
Peat	0.2	0.4	0.7	3.8	0.05	0.1	0.18

Source Marquez et al Ground thermal diffusivity calculation by direct soil temperature measurement.